JOURNAL OF GEOPHYSICAL RESEARCH, VOL. 107, NO. D3, 4028, 10.1029/2001JD000709, 2002

Submillimeter-Wave Cloud Ice Radiometer: Simulations of retrieval algorithm performance

K. Franklin Evans
Program in Atmospheric and Oceanic Sciences, University of Colorado, Boulder, Colorado, USA

Steven J. Walter
Aerojet, Azusa, California, USA

Andrew J. Heymsfield and Greg M. McFarquhar
National Center for Atmospheric Research, Boulder, Colorado, USA

Received 3 April 2001; revised 24 July 2001; accepted 27 July 2001; published 9 February 2002.

[1] The Submillimeter-Wave Cloud Ice Radiometer (SWCIR), developed by the Jet Propulsion Laboratory to fly on the NASA DC-8, has ten channels from four receivers at 183, 325, 448, and 643 GHz. The SWCIR is designed to retrieve upper tropospheric cloud ice water path (IWP) and median mass equivalent sphere diameter (D_{me}). This paper describes the retrieval algorithm developed for the SWCIR, results from retrieval simulations, and the rationale for choosing the SWCIR frequencies. The retrieval algorithm uses Bayes theorem to combine prior information about atmospheric properties with radiative transfer simulations. The algorithm uses a precalculated database of stochastic cirrus/atmospheric profiles and corresponding simulated SWCIR brightness temperatures. Statistics of cirrus microphysics are derived from in situ cloud probe data obtained during midlatitude winter and tropical field experiments, and include correlations between temperature, particle size, and ice water content. The Bayesian algorithm effectively interpolates between database cases that approximately match the observed SWCIR brightness temperatures. Retrieval experiments are performed for midlatitude winter ice clouds with the SWCIR viewing downward from 12 km and for tropical anvil cirrus with the SWCIR viewing upward from 10 km. Each experiment simulates SWCIR brightness temperatures (with 1 K added noise) from 10000 random cloud/atmosphere profiles. For clouds with IWP greater than 5 g/m^2 (which contain 97% of the simulated total ice mass) the overall median retrieval error is about 30% for IWP and 15% for D_{me}. The effects of liquid clouds just below ice clouds and of nonspherical ice particle shapes are small. *INDEX TERMS:* 3360 Meteorology and Atmospheric Dynamics: Remote sensing; 0320 Atmospheric Composition and Structure: Cloud physics and chemistry; 3394 Meteorology and Atmospheric Dynamics: Instruments and techniques; *KEYWORDS:* submillimeter, microwave, cirrus, remote sensing

1. Introduction

[2] There is an unmet need for global remote sensing of vertically integrated ice cloud mass for climate studies [*Wielicki et al.*, 1995]. Many global climate models now use prognostic cloud mass content schemes to improve their representation of cloud feedbacks [e.g., *Smith*, 1990; *Del Genio et al.*, 1996; *Fowler et al.*, 1999; *Lohmann and Roeckner*, 1996; *Rotstayn*, 1997; *Rasch and Kristjansson*, 1998; *Sud and Walker*, 1999]. An important component of these GCM microphysical parameterizations is the ice particle size, which determines the cloud radiative effect per mass and the ice cloud lifetime (through the particle fallspeed). Global measurements of vertically integrated cloud ice mass (ice water path or IWP) and particle size are therefore important for evaluating GCM cloud parameterizations.

[3] Existing satellite remote sensing techniques are inadequate to accuratel y measure cloud ice mass. Thermal infrared methods [e.g., *Ou et al.*, 1993; *Giraud et al.*, 1997; *Stubenrauch et al.*, 1999] saturate for moderate optical depths, require the cloud temperature to be known, and can only determine particle size (and hence IWP) for small crystal sizes. Visible and near-infrared solar reflection methods [e.g., *Rossow and Schiffer*, 1999; *Minnis et al.*, 1993; *Rolland et al.*, 2000] cannot distinguish ice from water cloud optical depth, can't measure low optical depth clouds over brighter land surfaces, and only work during daytime. Solar techniques also retrieve particle sizes near cloud top (leading to overestimation of the IWP due to the small particle bias), and are highly sensitive to nonspherical particle shape (because the phase function is sampled at back and side scattering angles). Thus there is a need for new cirrus remote sensing methods with different physics to avoid some of these problems.

[4] The millimeter-wave and submillimeter-wave ice cloud remote sensing technique has been developed over the past decade. *Gasiewski* [1992] performed a theoretical study on the sensitivity of frequencies up to 410 GHz to water vapor, precipitation, and liquid and ice clouds. *Evans and Stephens* [1995] extended the theoretical investigations by considering nonspherical ice particles at frequencies up to 340 GHz, and showed that the brightness temperature depression depends strongly on particle size and ice water path. They suggested that retrievals of both particle size and ice water path could be done with multiple widely spaced frequencies. In another theoretical study, *Evans et al.* [1998] modeled brightness temperatures up to 880 GHz from observed particle size distributions and several nonspherical ice particle shapes. The effect of absorption by water vapor was considered, and the use

0148-0227/02/2001JD000709$09.00

of a 183 GHz frequency with matched water vapor transmission was proposed to provide the upwelling atmospheric emission background. A simple two channel algorithm operating on brightness temperature depression was used to estimate the retrievals errors due to particle shape and size distribution. Variable height ice clouds, vertically nonuniform cirrus clouds, liquid water clouds, and atmospheric variability were not considered. Studies using actual measurements have been limited by the lack of submillimeter data. The Millimeter-wave Imaging Radiometer (MIR) [*Racette et al.*, 1996] with frequencies at 89, 150, 183, and 220 GHz has been used in several studies. *Deeter and Evans* [2000] and *Liu and Curry* [2000] used MIR channels at 150 and 220 GHz and *Weng and Grody* [2000] used MIR channels at 89 and 150 GHz to retrieve IWP and particle size in tropical cirrus anvils. *Wang et al.* [2001] analyzed MIR data with a new channel at 340 GHz and observed significant brightness temperature depressions from Arctic cirrus. The only reported measurements of ice clouds above 400 GHz have been taken with the Far InfraRed Sensor for Cirrus (FIRSC), which is a Fourier Transform Spectrometer with a cryogenic bolometer detector [*Vanek et al.*, 2001].

[5] Water vapor in the lower atmosphere emits submillimeter-wave radiation upward. If a cirrus cloud is above the lower troposphere, it scatters some of the submillimeter radiation in all directions. For a downward looking radiometer above the cirrus cloud, the scattering decreases the brightness temperature compared to that from clear sky. For an upward looking radiometer flying below the cirrus cloud, the ice cloud scattering increases the brightness temperature, as upwelling radiation is reflected downward by the cloud. The amount of scattering depends on the ice water path and the characteristic particle size relative to the wavelength of radiation. For a fixed ice mass there is usually a greater brightness temperature change for larger ice particles or higher measurement frequencies.

[6] These principles are illustrated in Figure 1 which shows calculated brightness temperature spectra up to 1000 GHz. The two basic scenarios modeled in this paper are simulated: downward viewing in a midlatitude winter atmosphere and upward viewing in a tropical atmosphere (these are the mean atmospheres described in section 4.2). As the water vapor absorption generally increases with frequency, the clear-sky brightness temperature for downward viewing decreases, while the upward viewing T_b increases. The change in brightness temperature from clear sky increases as the particle size is changed from D_{me} = 100 μm to D_{me} = 200 μm, but the fractional change is much larger around 325 GHz than at 643 GHz. This differential response to particle size allows widely spaced submillimeter frequencies to independently determine the ice water path and median mass ice particle diameter.

[7] Submillimeter radiation is also quite sensitive to water vapor in the middle and upper troposphere, which affects the clear-sky brightness temperature. Therefore a lower, millimeter-wave frequency that is less sensitive to small ice particles, but as sensitive to water vapor, may be used to correct for uncertainties in the water vapor behind the cloud. For downward viewing, water vapor absorption in and above the cloud reduces the sensitivity of submillimeter radiation to the ice cloud. This is the water vapor screening effect. It is illustrated in Figure 1a, which shows that the brightness temperature depression above 500 GHz is reduced when the cloud top altitude is changed from 10 km to 8 km. A submillimeter radiometer and retrieval algorithm must be able to correct for the reduced sensitivity due to water vapor screening.

[8] The purpose of this paper is to introduce the Submillimeter-Wave Cloud Ice Radiometer (SWCIR) and describe its expected accuracy for ice cloud retrievals. The SWCIR is designed to retrieve the ice water path and the characteristic ice particle size (here we use the median equivalent mass sphere diameter D_{me}). The SWCIR retrieval simulation system, including an operational retrieval algorithm and a new method for simulating realistic ice clouds from in situ microphysical observations, is described. Another purpose of this paper is to illustrate the method used for selecting the SWCIR frequencies, which may prove useful for other submillimeter radiometers under development.

2. Submillimeter-Wave Cloud Ice Radiometer

[9] The SWCIR measures thermal radiation emitted by the atmosphere in four discrete millimeter and submillimeter-wave frequency bands. Its primary goals are to validate the use of radiometry to quantitatively characterize cirrus and develop and demonstrate the technology needed to realize a low-cost, light weight, spaceborne cloud ice radiometer. The SWCIR, funded by NASA Instrument Incubator Program (IIP), was developed at the Jet Propulsion Laboratory.

[10] SWCIR cirrus retrieval products will be validated with those obtained from independent observations. Since concurrent millimeter-wave cloud radar data is complementary and well-suited for validation studies, the SWCIR was designed to fly on the NASA DC-8 along side the JPL/University of Massachusetts' 94-GHz cloud radar. This combination of sensors in conjunction with overflights of ground-based cloud observation facilities, such as the Atmospheric Radiation Measurement sites, will provide rich data sets for retrieval investigations.

[11] The SWCIR instrument requirements, listed in Table 1, are derived from these validation and technology development needs. SWCIR is designed to scan cross track from the NASA DC-8 as shown in Figure 2. An external mirror, mounted outside the aircraft, allows the radiometer to scan from zenith to near-nadir. (The airplane fuselage partially obstructs the nadir view.) As is shown in the figure, the external mirror assembly is motor-driven and is housed within a fairing to reduce drag forces.

[12] The reflected atmospheric emissions pass through an aircraft window made from high-density polyethylene, chosen because of its low loss and high strength. It is tapered from top to bottom to inhibit the formation of standing waves between the external and internal window surfaces. Without the taper, temperature changes inside and outside the aircraft would induce changes in window thickness that would modulate the phase of the standing wave pattern. This would appear as a time-variable change in the effective window transmission characteristics. Since this etalon effect is not limited to the aircraft window, the SWCIR optical design does not contain any parallel surfaces that could support standing waves.

[13] After passing through the window, a periscope transfers the atmospheric radiation down to the level of the optical table where it relayed through a series of high-pass, dichroic filters to each of the four receivers. The primary periscope mirror is motor-driven to rapidly steer the radiometer between views of the sky and the ambient and liquid nitrogen calibration targets. These targets are used to track short-term variations in radiometer gain. When combined with external tip curve calibrations [*Gatti et al.*, 1994], the SWCIR should be able to meet its 1 K absolute calibration requirement.

[14] As shown in Figure 3, the optical table has a planar layout that facilitates operations and troubleshooting. The optical table is mounted on two NASA DC-8 instrument racks and meets NASA DC-8 airworthiness requirements. Long optical paths were needed to both achieve the 1.5 degree beam width given the limits on the window size and reduce the sensitivity of the radiometric measurement to vibration and optical misalignment. Additionally, the internal optics were designed with 40 dB tapers to reduce spillover effects to negligible levels.

[15] A K-mirror polarization rotator sits at the entrance of the 643 GHz receiver [*Johnson*, 1977]. Rotating the K-mirror 45 degrees rotates the polarization of the incoming radiation by 90 degrees. Since the receivers are linearly polarized, the K-rotator rotates the polarization of the received radiation. This capability

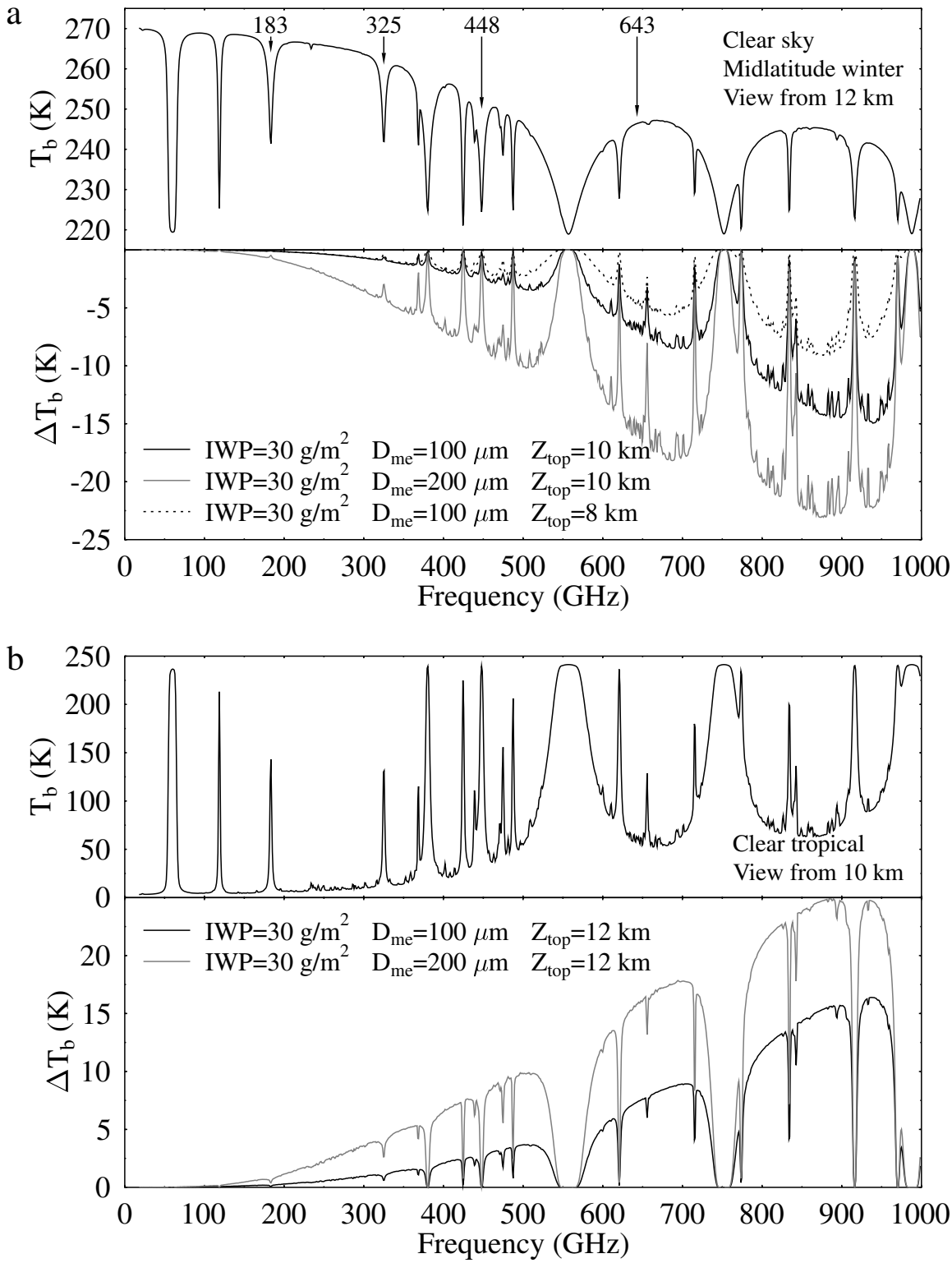

Figure 1. Simulated clear-sky brightness temperature (T_b) spectra and difference from clear-sky (ΔT_b) for various modeled ice clouds: (a) viewing downward at 30° from 12 km in the mean midlatitude winter atmosphere, and (b) viewing upward at 0° from 10 km in the mean tropical atmosphere. The ice clouds have different ice water path (IWP), median mass equivalent sphere diameter (D_{me}), and cloud top height (Z_{top}). All are uniform and 2 km thick. The SWCIR receiver central frequencies are shown with arrows. The surface emissivity is unity.

Table 1. SWCIR Specifications

	Specifications
Receiver center frequencies	642.86 GHz, 448.00 GHz, 325.15 GHz, 183.31 GHz
Band-pass center frequencies	642.86 ± 6.50; 448.00 ± 1.44, ± 3.00, ± 7.20; 325.15 ± 1.50, ± 3.18, ± 5.94; 183.31 ± 1.47, ± 2.85, ± 4.50
Brightness temperature precision	<0.5K
Brightness temperature accuracy	<1.0K
Radiometer system noise	<4000K
Radiometer beam width	1.5° 3dB FWHM
Beam pattern match with radar	<10%
Beam coalignment	0.15°
Elevation scanning range	−70° to +90°
Receiver polarization	linear
Orthogonal polarization	available at 643 GHz
Internal calibration	ambient target and cold load
External calibration	tip curves

enables investigations of polarization effects introduced by variations in crystal habits. The highest frequency channel was chosen for these measurements because the brightness temperature polarization effect increases with frequency.

[16] The receivers use Planar-Schottky mixers and multiplied-Gunn diodes for local oscillators [*Siegel et al.*, 1998]. The 643 GHz receiver is shown in Figure 4. Ambient temperature Schottky receivers were selected for SWCIR because the technology is directly applicable to future space systems. Currently, the maximum frequency for this receiver technology is roughly 650 GHz. Above 650 GHz, it becomes increasingly difficult to obtain sufficient local oscillator power to pump the front-end mixers without resorting to cryogenic systems or laser-pumped sources. These technologies are not attractive for space applications because the requisite hardware is large, heavy and power-intensive. Since the aircraft thermal environment can vary by more than 20° C, the receivers are insulated and temperature-controlled to minimize temperature-induced gain drifts.

[17] The choice of frequencies balanced sensitivity to ice mass and particle size with technological constraints posed by the choice of technology. The highest frequency selected for SWCIR was 643 GHz to take advantage of an existing design developed for the EOS Microwave Limb Sounder [*Waters et al.*, 1999]. This approach reduced both cost and risk. The other three frequencies were chosen to coincide with water vapor spectral lines at 183 GHz, 325 GHz, and 448 GHz. Since heterodyne receivers have limited bandwidth (>3%), locating the center frequency on narrow emissions lines allows the use of a single receiver front-end with multiple IF band passes to collect data at several opacities. The 183 GHz line was chosen because the receiver band pass could be adjusted to match its weighting function to the 643 GHz channel. The ability to match the higher frequency weighting functions combined with its relative insensitivity to cirrus allows it to correct for variations in the water vapor-induced emission background. The 325 GHz and 448 GHz water vapor lines were chosen for their opacity and their roughly equal spacing between 183 GHz and 643

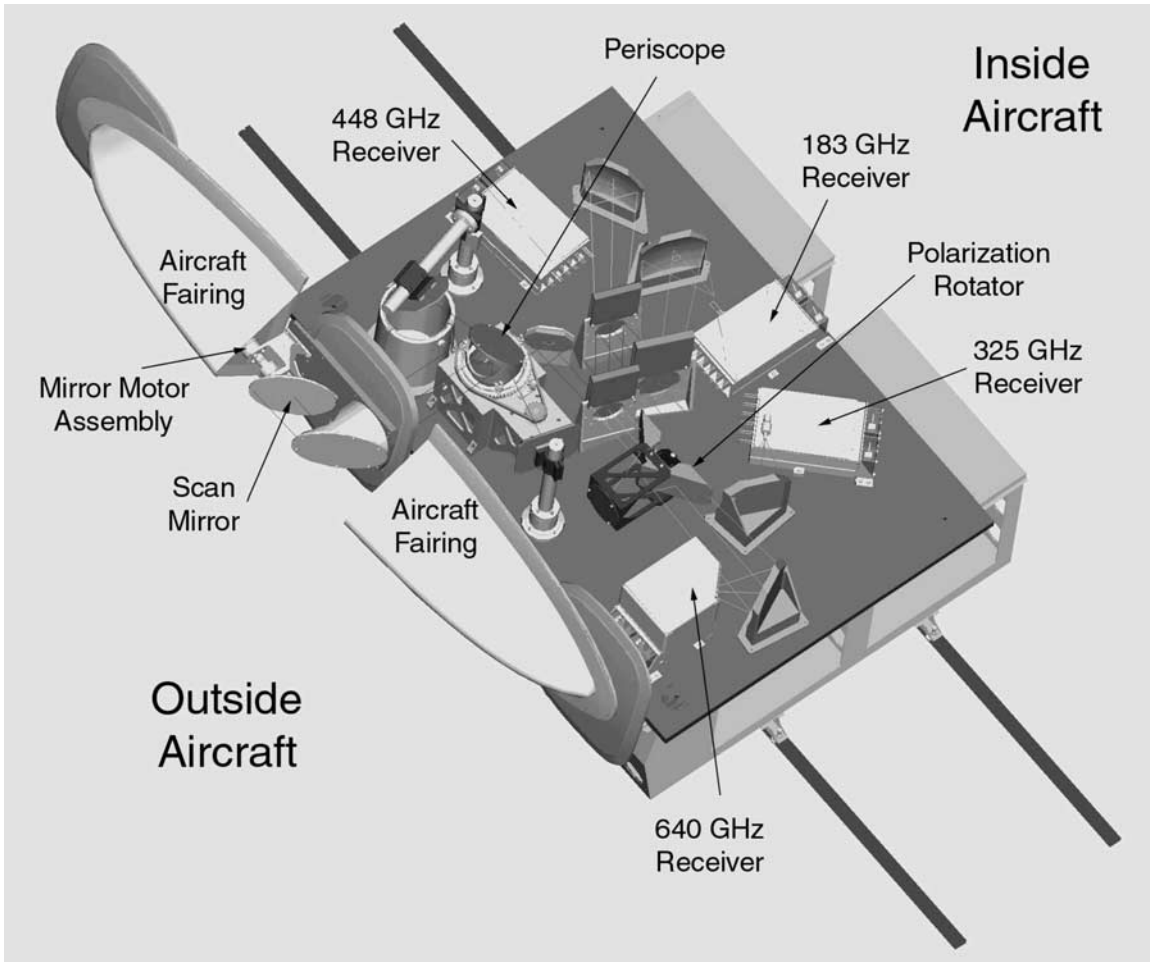

Figure 2. The SWCIR design viewed from the outside of the DC-8 aircraft.

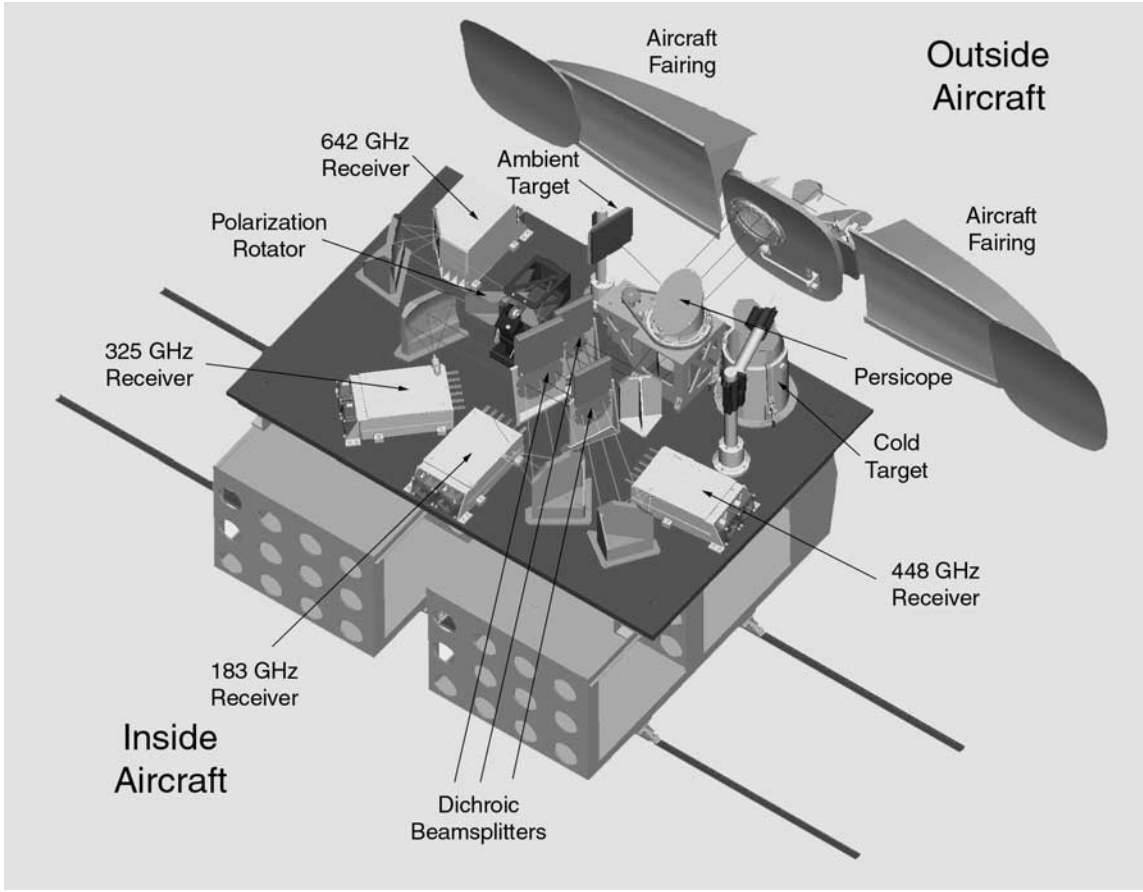

Figure 3. The SWCIR design viewed from the inside of the DC-8 aircraft.

GHz (which is desired for cirrus retrievals). Finally, a set of three band passes were selected for each of the 183 GHz, 325 GHz, and 448 GHz receivers. The method for choosing these frequencies is discussed in section 6.

[18] The receiver outputs are digitized along with a variety of instrument health and status data such as temperatures and voltages measured at a variety of components and motor positions. These data will be integrated with aircraft data including GPS time, aircraft orientation, and position. The data acquisition system uses a commercial-off-the-shelf (COTS) hardware and software providing a quick-look, real-time display in addition to archiving raw data for detailed analysis at a later date.

3. Bayesian Retrieval Algorithm

[19] The retrieval algorithm is designed primarily to derive cloud ice water path (IWP) and median mass particle diameter (D_{me}) from SWCIR brightness temperatures. However, it can also retrieve other properties, such as ice cloud height and the water vapor profile. The Bayesian retrieval algorithm uses a database of precalculated brightness temperatures for many cloud and atmosphere cases, and integrates over the points in the database with Bayes theorem. Bayesian inversion methods formally add prior information to that provided by the measurements to obtain a well posed retrieval and corresponding uncertainty estimate [*Sivia*, 1996]. Bayes theorem can be stated mathematically for the retrieval problem as

$$p_{\mathrm{post}(\mathbf{x}|\mathbf{T})} = \frac{p_f(\mathbf{T}|\mathbf{x})p_p(\mathbf{x})}{\int p_f(\mathbf{T}|\mathbf{x})p_p(\mathbf{x})d\mathbf{x}},$$

where $\mathbf{x}$ is the vector of cloud and atmosphere parameters that affect the measured brightness temperatures, $\mathbf{T}$ is the vector of measured brightness temperatures, $p_p(\mathbf{x})$ is the prior probability density function (pdf) of the cloud/atmospheric state $\mathbf{x}$, $p_f(\mathbf{T}|\mathbf{x})$ is the conditional pdf of the brightness temperature given the atmosphere vector (related to the forward radiative transfer model), and $p_{\mathrm{post}}(\mathbf{x}|\mathbf{T})$ is the posterior pdf of the cloud/atmospheric state

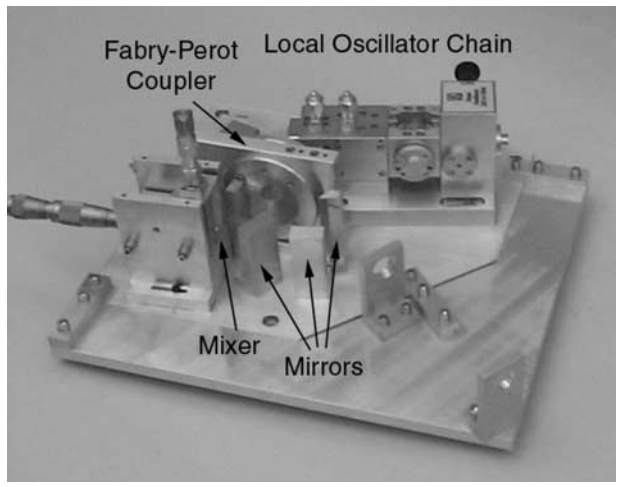

Figure 4. The 643 GHz receiver. A Fabry-Perot interferometer is used to couple the local oscillator into the mixer.

given the measured brightness temperatures. The prior pdf represents our knowledge of the atmosphere and cirrus clouds before the measurements are taken.

[20] The retrieved cloud/atmosphere state $\mathbf{x}_{ret}$ is calculated by integrating over the posterior pdf to find the mean state:

$$\mathbf{x}_{ret} = \int \mathbf{x} p_{\text{post}}(\mathbf{x}|\mathbf{T}) d\mathbf{x}.$$

In practice, this integral is replaced by a sum over the cases in the database:

$$\mathbf{x}_{ret} = \sum_i \mathbf{x}_i p_{\text{post}}(\mathbf{x}_i|\mathbf{T}).$$

This is a Monte Carlo integration because the database points are chosen randomly. One advantage of the Bayesian framework is that the uncertainties in retrieved parameters are naturally defined by the variance of the posterior pdf:

$$\sigma_x^2 = \int (x - \bar{x})^2 p_{\text{post}}(\mathbf{x}|\mathbf{T}) d\mathbf{x},$$

where σ_x is the one sigma error bar in x and $\bar{x} = x_{ret}$ is the mean x of the posterior pdf.

[21] The conditional pdf $p_f(\mathbf{T}|\mathbf{x})$ is the probability density of the brightness temperature vector given an atmospheric state. This is easily related to the forward radiative transfer function $\mathbf{T}_0 = \mathcal{R}(\mathbf{x})$, in that the probability density of $\mathbf{T}$ should be localized around $\mathbf{T}_0$. We assume a multivariate normally distributed probability density representing the uncertainty about $\mathbf{T}_0$:

$$p(\mathbf{T}|\mathbf{x}) = \prod_{j=1}^{M} \frac{1}{\sqrt{2\pi\sigma_j^2}} \exp\left[-\frac{\left[T_j - R_j(\mathbf{x})\right]^2}{2\sigma_j^2} \right],$$

where T_j is the j'th channel in the brightness temperature vector $\mathbf{T}$, $R_j(\mathbf{x})$ is the radiative transfer simulation for channel j, and σ_j is the standard deviation for channel j. This formulation assumes that the uncertainty in each channel is independent of the other channels, which is a good assumption for random measurement noise, but may be less viable for representing the radiative transfer modeling error. We assume that the uncertainty σ_j is due to the SWCIR absolute measurement errors. Since the conditional distribution is effectively zero if the brightness temperature vector is far from the observed one, the Bayesian algorithm interpolates between those points in the database that are reasonable matches to the observations.

[22] The prior probability distribution is a way of introducing other known information about the clouds or atmosphere. For example, we know that certain ranges of particle size are reasonable for cirrus clouds and that there is some correlation between temperature, particle size, and ice water content. If a remote sensing inversion is not completely well posed, then the addition of a priori information can serve as a constraint. In addition, the prior distribution gives a good indication of how to choose the random cases for the database. In fact, by choosing the database points in parameter space $\mathbf{x}_i$ distributed according to the prior pdf, the Monte Carlo integration simplifies to

$$\mathbf{x}_{ret} = \frac{\sum_i x_i p_f(\mathbf{T}|\mathbf{x}_i)}{\sum_i p_f(\mathbf{T}|\mathbf{x}_i)} \quad \mathbf{x}_i \text{ from } p_p(\mathbf{x}).$$

[23] The amount of information added by the observation can be defined from probability theory using the relative entropy concept [*Bernardo and Smith*, 1994]. The relative entropy is

$$I = \int p_{\text{post}}(\mathbf{x}|\mathbf{T}) \ln\left[\frac{p_{\text{post}(\mathbf{x}|\mathbf{T})}}{p_p(\mathbf{x})} \right] d\mathbf{x}.$$

This can be computed easily by integrating over all database points if there are enough points with significant posterior probability density. If the observation adds no information then the posterior pdf equals the prior pdf, and the relative entropy is zero. The relative entropy is positive if the posterior pdf is narrower than the prior pdf. The relative entropy may be expressed in base 2 units or bits by dividing by ln 2.

[24] The sums in the Bayesian retrieval algorithm span all points in the database. Including all the database points wastes computation time calculating the conditional pdf for points where the pdf is effectively zero, (i.e., where the observed brightness temperature is far from that of the database case). The conditional pdf is the product of exponentials, and, thus, is also the exponential of χ^2:

$$\mathbf{x}_{ret} = \frac{\sum_i \mathbf{x}_i \exp\left[-\frac{1}{2}\chi_i^2\right]}{\sum_i \exp\left[-\frac{1}{2}\chi_i^2\right]} \quad \mathbf{x}_i \text{ from } p_p(\mathbf{x}),$$

where χ^2 is a measure of the difference between the observed and database brightness temperature vector

$$\chi_i^2 = \sum_{j=1}^{M} \frac{\left[T_j - R_j(\mathbf{x}_i)\right]^2}{\sigma_j^2}.$$

One way to speed up the Bayes integration is to stop the χ^2 summation and not calculate the posterior pdf when the χ^2 exceeds a maximum, user specified value, $\chi^2 > \chi^2_{max}$. A second method is to avoid database points that are likely to have a large χ^2. The database can be sorted to use only those points that lie within in a particular range around the observed brightness temperature vector. The brightness temperature space is multidimensional with ten SWCIR channels, and cannot be sorted in all dimensions. Instead, a linear combination of channels having the maximum variance (i.e., the first principal component) is used to sort the database points. When doing retrievals, the observed brightness temperature vector is projected to the first principal component, which locates the observation along this one-dimensional sorted list of database points. The square root of the χ^2_{max} cutoff then gives the principal component range (above and below the observation) to use. It can be shown that while this method includes many points with larger χ^2, it does not exclude any points with smaller χ^2. If there are no database points within this cutoff, then the closest database point is used for the retrieval.

4. Atmosphere and Ice Cloud Simulation Method

[25] There are two parts to generating the database for input to the Bayesian retrieval algorithm: (1) creating the random atmosphere and cirrus cloud properties, and (2) computing the simulated SWCIR brightness temperatures. The temperature, humidity, and cloud properties are distributed in the database according to the Bayes prior probability density function. This distribution represents our estimate of the "climatology" of cirrus cloud properties, including the relationships between parameters, such as ice water content and particle size. In this study the focus is on midlatitude winter synoptically generated ice clouds and tropical convective anvil cirrus.

[26] The procedure for creating the random clouds and atmospheres is described below. The database is typically developed for one geographic region and season. The retrieval database should

contain the full range of relevant atmospheric/cloud situations. Any parameter that significantly affects the brightness temperatures should be varied in a realistic manner.

4.1. Ice Cloud Microphysics Data

[27] In situ observed cirrus microphysical data are used to create a realistic distribution of ice cloud properties. The microphysical information is obtained from Particle Measuring Systems (PMS) 2DC and 2DP probes flown in two different field experiments. These probes observe the particle shadow from which particle projected area and maximum projected diameter are obtained. The area ratio (A_r) is the ratio of the projected area to the area of the circumscribing circle of the maximum diameter (D_{max}).

[28] For midlatitude winter synoptic ice cloud simulations we use 2DC and 2DP data obtained during the FIRE-I [*Starr and Wylie*, 1990] experiment in October, 1986 by *Heymsfield et al.* [1990]. Spiral descents from four flights of the King Air aircraft, with altitudes ranging from 8.7 km to 5.3 km, produced 695 five second samples. The FIRE-I microphysics data indicated that most of the particles were rosettes. A new area ratio-effective density (A_r-ρ_e) relation [*Heymsfield et al.*, 2002] appropriate for 5 bullet rosettes is employed. The A_r-ρ_e relation and the definition of effective density, $m = (\pi/6)D_{max}^3 \rho_e$, are used to convert the particle concentration as a function of maximum diameter and area ratio to a particle mass distribution ($n(m)$) for each sample. The 2DC probes underestimate the particle concentration for maximum diameters below 100 μm [*McFarquhar and Heymsfield*, 1996]. A new parameterization for the small particle size distribution, developed by Nari Orikasa and Andy Heymsfield, is used. This parameterization is based on small particles observed in midlatitude winter synoptically generated cirrus in about 30 balloon ascents of the HYVIS microvideograph system [*Murakami and Matsuo*, 1988; *Mizuno et al.*, 1994]. The application of this parameterization made only small changes to the results because most of the ice mass is contained in the larger particles.

[29] For tropical anvil cirrus simulations we use 2DC probe data obtained during the Central Equatorial Pacific Experiment (CEPEX) in 1993 [*McFarquhar and Heymsfield*, 1996]. In CEPEX the 2DC probe flew on a Learjet with a maximum altitude of 14 km. There are 12,505 10 second samples, each having the particle number concentration as a function of maximum diameter and area ratio. The area ratio and maximum diameter are used to assign crystal habit, and hence mass to each of the bins [*Heymsfield et al.*, 1990]. The microphysics data are represented with a gaussian distribution of temperature (see section 4.2), so a subset of 3000 cloud probe samples was chosen to match a gaussian distribution with mean of 230 K and standard deviation of 15 K.

[30] The ice water content (IWC) and median mass equivalent sphere diameter (D_{me}) of each microphysical sample is obtained by finding the gamma distribution that matches the third and fourth moments of the equivalent sphere diameter, D_e [*Evans et al.*, 1998]:

$$M_N = \sum n_i \quad D_{e,i}^N D_e = \left(\frac{6m_i}{\pi\rho_i}\right)^{1/3}$$

$$IWC = \frac{\rho_i \pi}{6} M_3 \quad D_{me} = \frac{1 + 3.67}{5} \frac{M_4}{M_3}$$

using $\rho_i = 916 \mathrm{kg}/m^3$ for the density of ice. This assumes a gamma distribution with $\alpha = 1$, where $N(D_e) \propto D_e^{\alpha} \exp[-(\alpha + 3.67)D_e/D_{me}]$. *Evans et al.* [1998] showed that gamma size distributions defined in this way are almost equivalent to the actual distribution in terms of submm radiative transfer. Scatterplots of D_{me} versus temperature, IWC versus temperature, and IWC versus D_{me} are displayed in Figures 5 and 6. These show significant correlation between temperature and D_{me} and IWC and D_{me}. The statistics (mean, standard deviation, and correlation) derived from these data are the inputs to the cloud generation procedure.

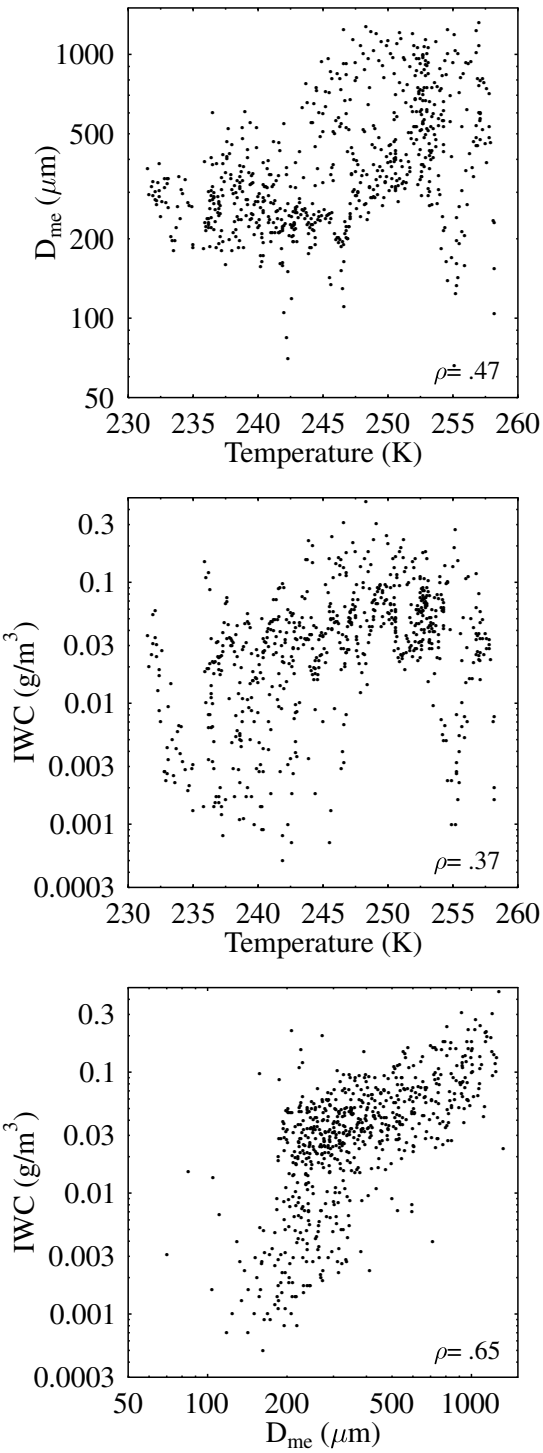

Figure 5. Scatterplots of temperature, ice water content, and median mass particle diameter from the FIRE-I data. The correlation coefficient ρ is listed.

4.2. Cloud and Atmosphere Simulation Procedure

[31] In situ cloud probes usually collect data along horizontal aircraft flight lines, and thus do not obtain the coherent vertical information needed for radiative transfer simulations. The hun-

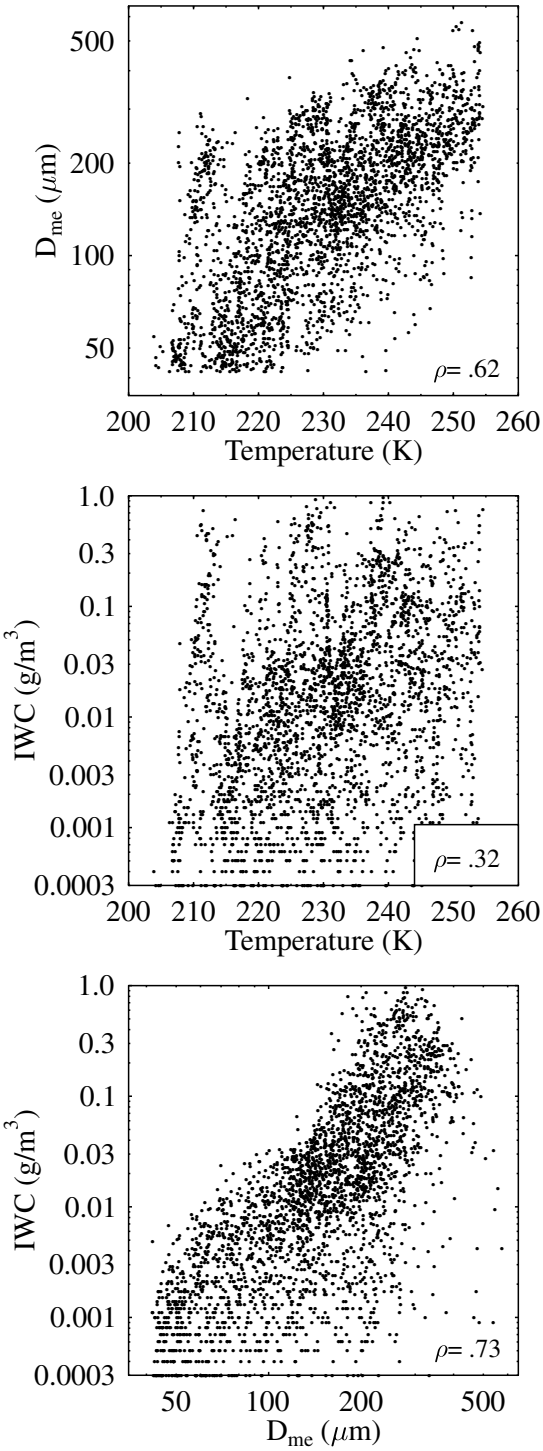

Figure 6. Scatterplots of temperature, ice water content, and median mass particle diameter from the CEPEX data.

dreds of Lagrangian spiral flights that would be required to define the cirrus profile statistics for the retrieval database are not available. The cloud probe data do show, however, the dependence of ice particle size and ice water content on temperature. Some assumptions must be made to construct the full range of realistic vertical profiles from the in situ data. Simply multiplying the IWC by the cloud thickness would not take into account the tendency for the IWC and D_{me} to decrease with height, both as the cloud height changes and within the cloud. The new approach developed here takes advantage of the correlation of temperature, IWC, and D_{me} from the cloud probe data to construct vertically inhomogeneous clouds based on the cloud top and base temperature. The method uses random sampling of probability distributions to generate clouds with stochastic properties.

[32] The first step is to generate random temperature and relative humidity profiles with the appropriate statistics. Many observed meteorological soundings that are representative of a particular experiment are selected. The covariance matrix and mean profile of temperatures and relative humidities at a set of altitudes (e.g., 1 km spacing) are calculated. A principal component or empirical orthogonal function (EOF) analysis determines the independent component profiles from the covariance matrix. A random profile is made by using independent gaussian noise, with variance of the eigenvalues, for the principal component amplitudes. With this method the random temperature and relative humidity profiles have the same mean, standard deviations, and vertical correlations as the set of observed profiles.

[33] The simulations presented here used profiles from the TIGR3 database [*Chedin*, 1985]. The midlatitude simulation used 72 TIGR3 profiles from 35 to 50N latitude in the December to February season. The tropical simulation used 118 profiles from 15S to 15N latitude. The mean and variability of the temperature and relative humidity profiles from 10,000 realizations are shown in Figure 7. As expected, there is a larger temperature variability for midlatitude winter than for tropical atmospheres.

[34] The stochastic clouds are constructed in a series of steps. The cloud top height has a gaussian distribution, which agrees with mm cloud radar top height distributions from the tropical west Pacific and wintertime Oklahoma (not shown). The mean cloud top height is specified in terms of temperature and thus depends on the randomly created temperature profile. There may be one or two cloud layers, though only single cloud layers are used here. The geometrical thickness has an exponential distribution. The random cloud is rejected if the thickness is less than 50 m or the cloud bottom is below a specified minimum altitude. These probability distributions are independent.

[35] The ice cloud top and bottom temperatures are used to generate random values of IWC and D_{me} at cloud top and bottom from the covariance matrix of observed temperature T, IWC, and D_{me}. Lognormal distributions of IWC and D_{me} are assumed, resulting in a trivariate gaussian distribution of T, ln(IWC), and ln(D_{me}). Table 2 lists the parameters of the trivariate gaussian distribution from the FIRE-I and CEPEX microphysics data. Fixing the temperature results in a bivariate gaussian distribution of ln(IWC) and ln(D_{me}) (with temperature dependent means). Gaussian random numbers are used to generate the random ln(IWC) and ln (D_{me}) that are correlated with temperature (and each other).

[36] The modeled ice cloud is completely specified by the IWC and D_{me} at the top and bottom. A linear profile of D_{me} in the cloud is assumed. If the D_{me} at cloud top is larger than at cloud base, that random cloud is rejected (it must also be in the range of the scattering tables from 10 to 1000 μm). The ice water content inside the cloud is interpolated according to IWC $\propto D_{me}^{b}$. The exponent b is derived from the top and bottom values of IWC/D_{me}, and cases with $b < 0$ are rejected. The ice water path is calculated by integrating the IWC through the cloud depth, assuming the 0.5 km sublayers have uniform properties. The "mean" cloud D_{me} is obtained from the third and fourth moments of D_e as described in section 4.1. The gamma particle size distribution width parameter α is randomly chosen to be 0, 1, 2, or 7.

[37] Liquid clouds below ice clouds are allowed in the cloud generation scheme. An ice to liquid transition zone is specified in terms of temperature. For each cloud the ice/liquid transition temperature is randomly selected from a uniform distribution. The transition temperature is converted to height with the temperature profile and used to cut the cloud into separate ice and liquid

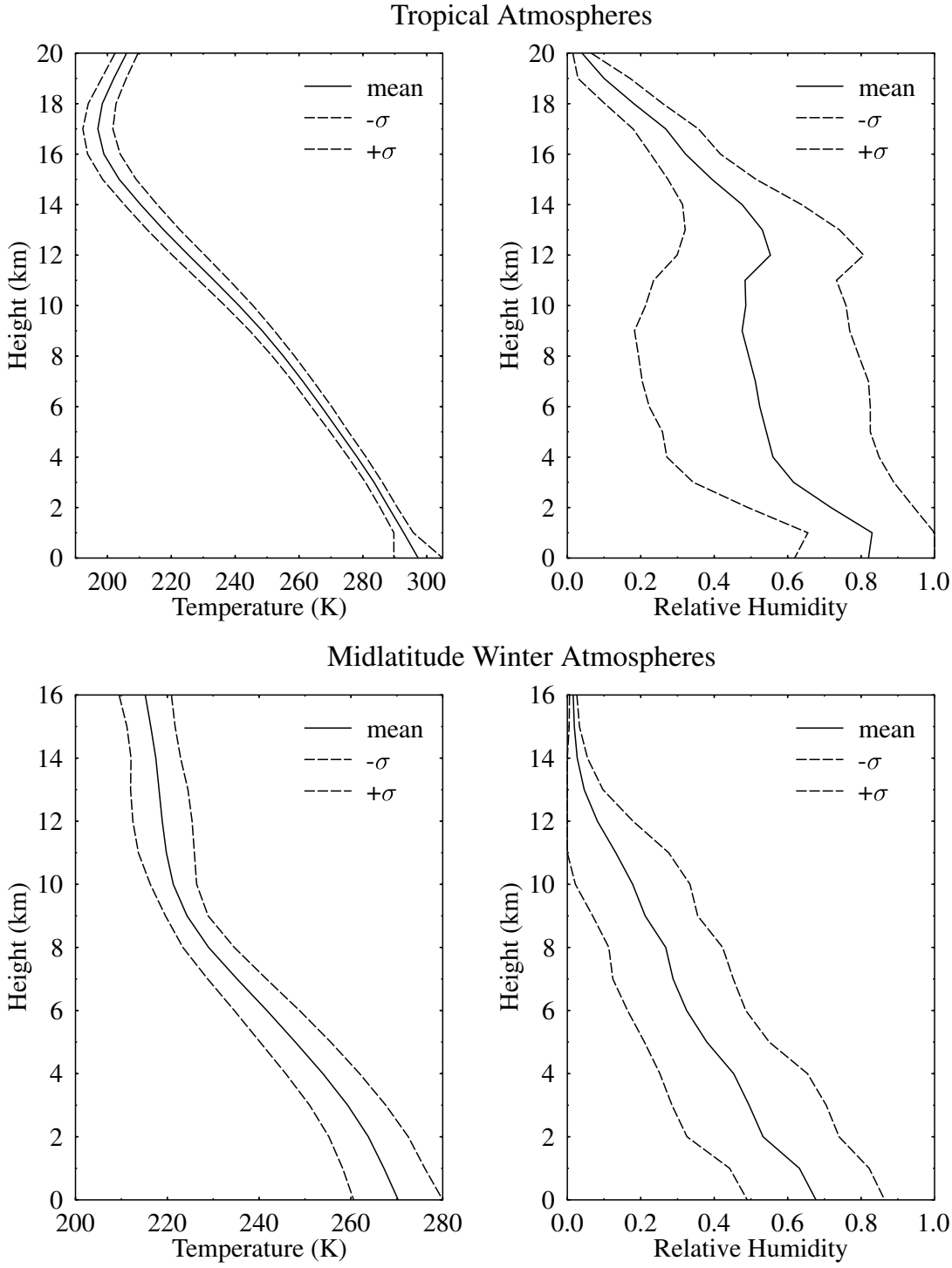

Figure 7. The mean and mean ± standard deviation profiles of temperature and relative humidity from 10,000 randomly generated profiles for the tropical and midlatitude winter simulations.

parts. Thus, mixed phase layers are not modeled, though the adjacent ice and liquid layers may be effectively mixed by the radiative transfer. The cloud liquid water content (LWC) is the same as the ice cloud base IWC. If the cloud top is below the transition level, then there is no ice portion and the LWC is set to 0.1 g/m^3. The liquid cloud D_{me} is set to 12 μm (this value is not important in the submm).

[38] The relative humidity inside liquid clouds is set to 100%. The mean relative humidity inside an ice cloud is set to ice saturation, but the actual relative humidity fluctuates with the random atmosphere generation process. The relative humidity is not allowed to exceed 100% or go below 0.01%.

4.3. Radiative Transfer

[39] The retrieval database consists of the desired retrieval parameters, such as IWP, D_{me}, and layer humidities, and the associated SWCIR brightness temperatures for many atmosphere/

Table 2. Mean and Covariance Matrix of the Ice Cloud Microphysics Parameters[a]

Variance	Mean	Covariance		
		Temperature	ln(IWC)	ln(D_{me})
		Midlatitude Winter/FIRE-I Microphysics		
Temperature	246.1	46.302	3.265	1.723
ln(WC)	−3.646	3.265	1.647	0.4537
ln(D_{me})	5.908	1.723	0.4537	0.2933
		Tropical/CEPEX Microphysics		
Temperature	230.3	138.78	7.833	4.258
ln(IWC)	−4.527	7.833	4.268	0.8855
ln(D_{me})	4.950	4.258	0.8855	0.3422

[a] The statistics are given for temperature (K), ice water content (g/m^3), and median mass equivalent sphere diameter (D_{me}, μm).

cirrus cases. For each random atmosphere/cloud case a radiative transfer model simulates the SWCIR brightness temperatures for desired viewing angles and aircraft altitudes.

[40] Owing to the large number of cases in the retrieval database, we have used an approximate, but computationally efficient Eddington second approximation/single scattering hybrid model [*Deeter and Evans*, 1998]. The current version of the model implements vertically inhomogeneous clouds with uniform sublayers, in this case of 0.5 km or smaller thickness. The accuracy of the model in comparison to a standard multi-stream model is a few percent in the brightness temperature change ΔT_b. A purely absorbing atmosphere outside the cloud layer is assumed. The surface temperature is set to the lowest atmosphere level, and the surface emissivity is set to unity (the SWCIR channels have small or no surface contribution).

[41] The single scattering information is tabulated as a function of frequency and D_{me} for input to the radiative transfer model. For solid spherical ice particles the scattering properties are calculated with Mie theory. The lower density of ice particles is accounted for to first order by using the equivalent mass sphere diameter to define the size distributions. The scattering tables may also be created for randomly oriented nonspherical particles. The index of refraction of ice in the scattering computations is obtained from *Warren* [1984].

[42] The molecular absorption (mainly from water vapor and oxygen with a small contribution from ozone) is calculated with the LBLRTM line-by-line model. Because a line-by-line model is too slow for creating the retrieval database, an interpolation approach is taken. Molecular absorption profiles are calculated for a base atmosphere and warmer (+3 K), drier (0% RH), and moister (100% RH) atmospheres. The base atmosphere has the mean temperature, water vapor, and ozone profile of the selected TIGR atmospheres up to 50 km. The molecular absorption for any arbitrary profile around the base case is interpolated accurately from the input absorption profiles. The clear-sky brightness temperature errors from this procedure are usually less than 0.2 K. The LBLRTM layer optical depths are computed for 0.5 km layers below 20 km (larger above) and are averaged spectrally to 1.0 GHz. Two monochromatic radiative transfer calculations are done for each SWCIR channel to simulate the double-sideband receivers. The error from using monochromatic calculations at the band-pass centers, rather than integration over the actual bandwidths, is negligible.

5. Retrieval Simulation Experiments and Results

[43] Retrieval simulations are performed to determine the accuracy of retrieving ice cloud and water vapor profile parameters with the SWCIR. These are done by simulating observations with a radiative transfer model. The simulated observations, including added measurement noise, are then input to the Bayesian algorithm to retrieve the desired parameters. Since this is a simulation, the "true" parameters values are known, and can be compared with the retrieved parameters to determine the retrieval accuracy. This has been done repeatedly for a realistic distribution of cloud and atmospheric parameters to make an estimate of the accuracy of the parameter retrievals. In order for the accuracy estimate to be reliable, all geophysical parameters that could influence the measured radiation need to be varied realistically. This study primarily uses the same microphysical statistics to generate the clouds for the simulated observations as are used in the prior probability distribution in the Bayes retrieval algorithm.

5.1. Retrieval Simulation Experiments

[44] Simulations are performed for two basic situations: ice clouds in midlatitude winter and cirrus anvils in the tropics. The temperature and relative humidity profile statistics and the ice and water cloud microphysics are described in section 4.2. The parameters that specify the cloud geometry distributions are listed in Table 3. The simulated SWCIR observations are generated with the same procedure as the retrieval database, but with a different random number generator seed and with noise added.

[45] The simulations in this section use the 10 SWCIR channels with frequencies given in Table 1. The SWCIR specification is 1.0 K absolute accuracy in brightness temperature, so gaussian noise of 1.0 K rms is added to each channel. The retrieval database consists of 3×10^5 cases and the χ^2 cutoff is 50.

[46] The flight altitude for the midlatitude winter simulation is 12 km which is near the DC-8 ceiling and above nearly all the simulated cloud tops. Since the SWCIR cannot view nadir, the viewing zenith angle is 30°. For the tropical simulation, the flight

Table 3. Parameters of the Probability Distributions Describing the Cloud Geometry

Parameter	Midlatitude Winter	Tropical
Temperature of mean cloud top height, K	235	218
Mean height of cloud top, km	7.0	13.0
Standard deviation of cloud top height, km	1.5	2.0
Mean cloud thickness, km	1.0	1.0
Minimum cloud base height, km	1.0	10.0
Ice/liquid transition zone, K	243–273	...

Table 4. Statistics of the Randomly Generated Ice Clouds[a]

Parameter	Mean	Median	Minimum	Maximum
		Midlatitude Winter Simulation		
IWP, g/m^2	31.7	11.0	0.03	2353
D_{me}, μm	327.6	300.4	54.7	932.6
Z_{top}, km	7.08	7.09	1.15	13.62
ΔZ, km	0.95	0.69	0.01	6.55
		Tropical Simulation		
IWP, g/m^2	27.2	4.42	0.00	9973
D_{me}, μm	125.1	109.8	17.6	738.3
Z_{top}, km	13.61	13.46	10.10	20.79
ΔZ, km	0.864	0.64	0.05	7.89

[a] IWP is ice water path, D_{me} is median mass equivalent sphere diameter, Z_{top} is cloud top height, and ΔZ is cloud thickness. The midlatitude winter statistics exclude the liquid only cases (3.0%).

altitude is 10 km. This is the minimum desired altitude given the upper tropospheric water vapor absorption in the tropics. The upward viewing geometry is simulated with a zenith angle of 0°. The minimum cloud altitude in the tropical simulation is 10 km, so the aircraft is assumed to be always flying below, not inside, the clouds.

[47] The statistics of the 10,000 randomly generated clouds used for testing are listed in Table 4. The typical midlatitude winter ice cloud has higher IWP and D_{me} than the typical tropical cloud. The width of the IWP distribution is wider for the CEPEX tropical microphysics, yielding a mean IWP that is similar for the two simulations. In the midlatitude winter simulation 7.6% of the cases contain both an ice and liquid cloud, while 3.0% of the cases have only a liquid cloud. Of the cases with both ice and liquid clouds, the mean and median liquid water paths are 86 and 32 g/m^2, respectively, which is reasonable for altostratus clouds.

[48] Many of the simulated ice clouds have an IWP that is too small for the SWCIR to measure accurately. However, for most climate applications, it is not the number of cloudy pixels that needs to be measured, but the total ice mass. Therefore a more relevant statistic is the fraction of the total ice mass that can be measured. The cumulative distribution of IWP by number of pixels and by total ice mass is shown in Figure 8. If we choose 5 g/m^2 as the threshold for measurable IWP, then 31.5% (midlatitude) and 52.3% (tropical) of the clouds fall below the threshold. However, only 2.3% (midlatitude) and 3.2% (tropical) of the total simulated ice mass is below the threshold.

5.2. Single Pixel Ice Cloud Retrieval Results

[49] The IWP and D_{me} retrieval errors are assessed by comparing the retrieved parameters to the known values. Traditionally, the error for quantities, such as IWP, that vary by orders of magnitudes is expressed in a fractional sense. Here we use the fractional or logarithmic difference expressed in decibels (dB). However, a fractional error for IWP near zero is meaningless, and thus the fractional error should only be considered for cases above the noise level. We apply the fractional error to cases with the IWP above a cutoff of 5 g/m^2. The often-used rms difference is easily skewed by a few very poor retrievals. Instead of the rms difference, we primarily use a more robust statistic, the median of the absolute value of the error. Thus, for all the retrievals being combined for an error estimate, 50% have a error less than the median error, and 50% have a larger error. For a zero mean gaussian distribution the root mean square error is 1.48 times the median absolute error. A 1 dB error is a factor of $10^{0.1}$ or about 25%, while a 3 dB error is a factor of 2.

[50] Figure 9 shows the median fractional error as a function of cloud top height for the two simulations. For the midlatitude winter simulation the median ice water path error ranges from near 1 dB for higher altitude clouds to about 2 dB for low-altitude clouds. Water vapor absorption prevents the higher SWCIR frequencies from sensing the lower troposphere, so most of the information for the lower altitude clouds is from the 183 GHz and 325 GHz channels. Many of the low-altitude, warmer clouds derived from the FIRE-I microphysics have higher IWP and larger particles, where the lower frequencies are most sensitive. The median error in D_{me} has less height dependence and is less than 1 dB for most altitudes. For the tropical simulation the median IWP error is around 1.0 dB for clouds tops below 14 km, but increases to 3.0 dB for the highest clouds. The SWCIR frequencies are relatively insensitive to clouds near the tropical tropopause, which have small particles and low IWP. Again, the median error in D_{me} is much smaller and does not vary significantly with height.

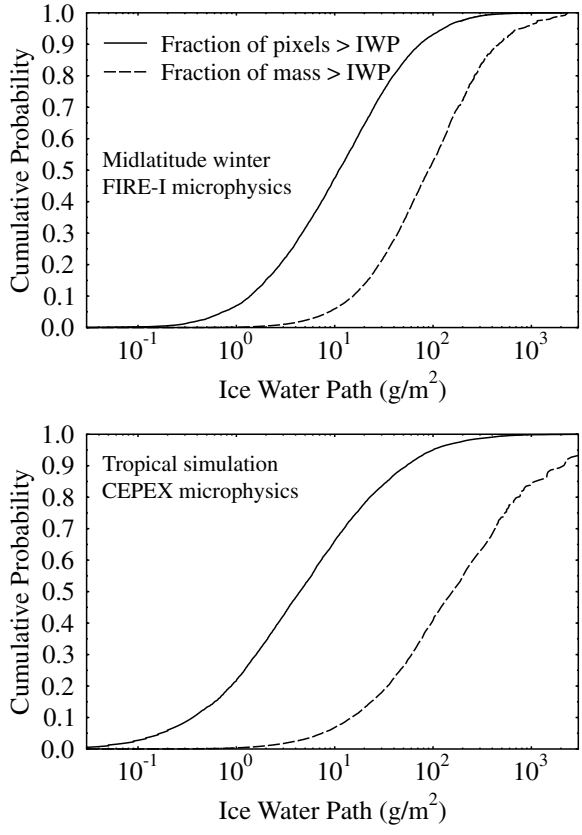

Figure 8. The fraction of pixels with IWP greater than a given value (cumulative distribution function) and the fraction of the total mass in pixels with IWP greater than a given value for the two simulations.

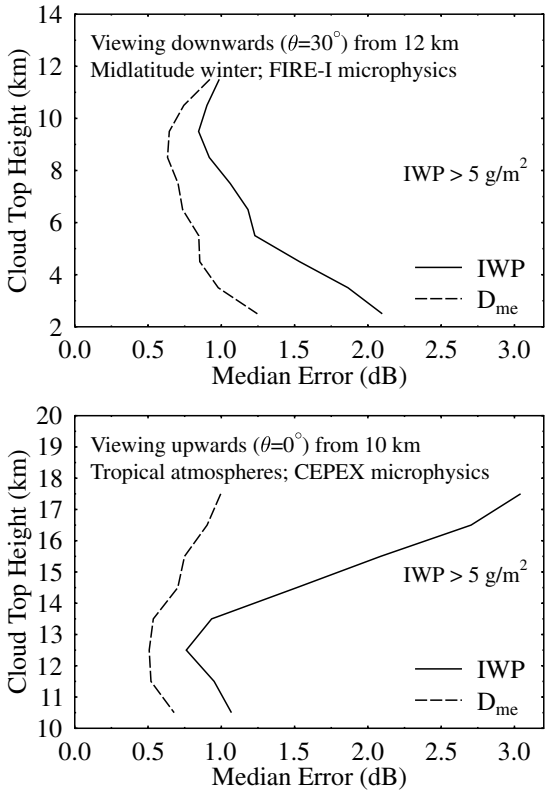

Figure 9. Median fractional error in dB of the retrieved ice water path and median mass diameter as function of cloud top altitude for the midlatitude winter and tropical simulations. Only cases with IWP greater than 5 g/m^2 are included.

[51] In many ways the bias error in cirrus retrievals is more important than the single pixel error because individual retrievals can be averaged to determine the ice mass in a region. Figure 10 shows the mean fractional difference (or bias) between the true and retrieved IWP and D_{me} as a function of cloud top height. For the midlatitude winter simulation the biases are small, mostly less than 0.5 dB. For the tropical simulation the IWP has a large negative bias for high altitude clouds, meaning that the average cloud with IWP > 5 g/m^2 has a retrieved IWP that is too small. In contrast, the retrieved D_{me} for the higher clouds is too large on average. Because of the small brightness temperature signal at SWCIR frequencies from the thin cirrus near the tropical tropopause, the retrievals are biased toward small IWP by the prior probability distribution.

[52] One strategy to increase the sensitivity to thin ice clouds is to view along a slant path, along which the SWCIR beam intersects a larger ice mass. Figure 11 compares IWP retrieval error for the standard viewing angles and slant paths of 70.5° (three times the zenith path length) as a function of ice water path. As expected, the near zenith retrieval error is large for low ice water path because the corresponding brightness temperature change is small. The retrieval errors for lower IWP are reduced with the slant viewing path. For the midlatitude winter simulation, the retrieval errors increase for the largest IWP. This happens because the brightness temperatures begin to saturate at high IWP and the large IWP clouds tend to occur at lower altitudes which are screened by water vapor absorption. Both these effects are increased with the slant path, and the midlatitude winter IWP retrieval error is substantially worse at high IWP for the slant path. The tropical simulation has small retrieval error at large IWP for both viewing angles. This different result occurs because the smaller particles reduce the brightness temperature saturation effect and water vapor screening is not a problem for upward viewing. The dip in the IWP error from 2 to 5 g/m^2 in the zenith view for the tropical simulation is caused by the large number of clouds in the prior probability distribution with their IWP in this range. This biases the low IWP retrievals toward these values because there is little brightness temperature signal at these low IWP.

[53] The overall single pixel fractional error for the two simulations and two view angles are shown in Table 5. The retrieval errors are quite low, with median IWP errors around 1 dB and rms IWP errors around 2 dB. This is encouraging because it is considerably better than existing remote sensing techniques. The median mass diameter rms errors are about 1.0 dB. These median fractional errors are for ice water paths above a 5 g/m^2 threshold. As shown in Figure 8, most of the ice mass exists in clouds with IWP greater than 5 g/m^2 (at least for these simulations, and probably in reality as well).

[54] One advantage of the Bayesian retrieval method is that error bars, defined by one standard deviations, are retrieved along with the parameter values. The retrieval simulations offer a means to test the accuracy of these error bars. A normalized error is defined by $\delta = (q_{ret} - q_{true})/\sigma_q$, where q_{ret} and q_{true} are the retrieved and true parameter values and σ_q is the retrieved standard deviation. This normalized error is only calculated when there are 10 database cases within the χ^2 cutoff. One would like the Bayesian error bars to mirror standard gaussian errors (though the error statistics are not necessarily gaussian), so that the error would be within one standard deviation in 68% of the cases. Table 6 lists the fraction of cases for which the normalized error is within ±1 and ±3. The normalized errors are within ±1 somewhat more often than, but close to, 68% of the time. The normalized error is within ±3 in 97% to 98% of the cases. This shows that the errors are somewhat nongaussian since a standard normal distribution is within ±3 fully 99.7% of the time.

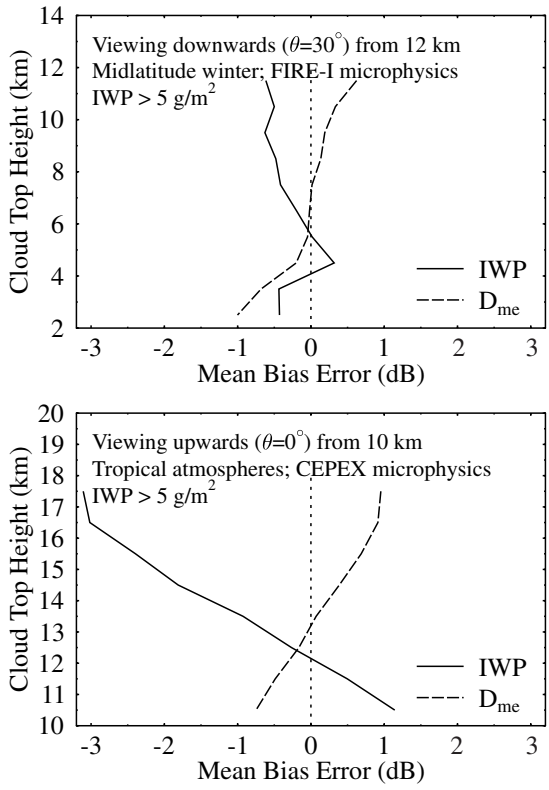

Figure 10. Mean bias fractional error in dB of the retrieved ice water path and median mass diameter as function of cloud top altitude for the midlatitude winter and tropical simulations.

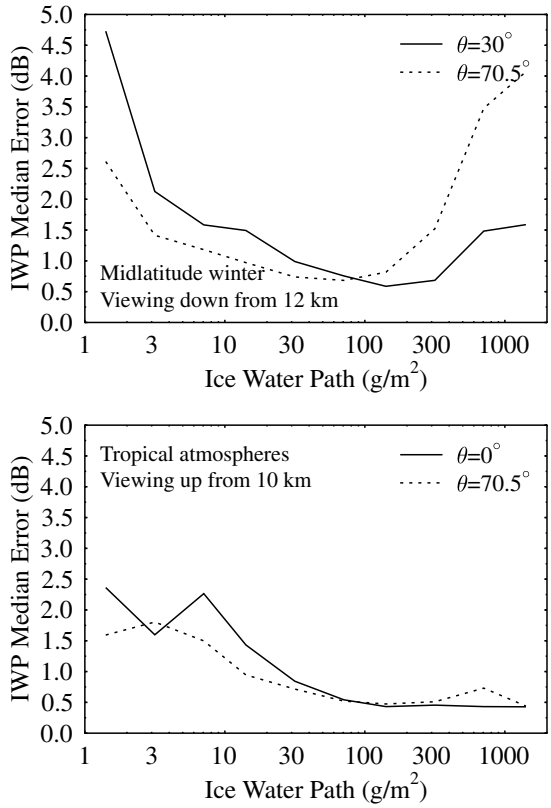

Figure 11. Median ice water path error as a function of IWP for two viewing angles for the midlatitude winter and tropical simulations.

[55] The relative entropy is a measure of how much the uncertainty in all the parameters is reduced by one SWCIR measurement. The median relative entropy over all simulated observations (with more than 10 database points within the χ^2 cutoff) is 8.8 bits for the midlatitude winter simulation and 8.9 bits for the tropical simulation. One bit of information reduces the uncertainty by a factor of two, 2 bits by a factor of 4, etc. The amount of information added by the SWCIR measurements varies with the cloud case from 5.4 bits to 18.2 bits (limited by the size of the database). Another way to express this is that the volume of parameter space is reduced from the prior pdf to the posterior pdf typically by a factor of $2^{8.9} = 470$.

[56] The effect of liquid clouds in the midlatitude winter simulation can be seen by analyzing the retrieval accuracy for cases containing only ice clouds with those containing both ice and liquid. Figure 12 plots the IWP and D_{me} median retrieval error as a function of cloud bottom altitude for three sets of cases. There is no liquid cloud in 89.4% of the cases, and both ice and liquid clouds in 7.6% of the cases (3.0% have liquid, but no ice). There is very little difference in retrieval accuracy between the ice only and ice + liquid cases, except for a small increase in median IWP error for ice cloud bases between 4 and 5 km. We conclude that liquid clouds do not dramatically affect the ice cloud retrievals. While this is not an explicit test of mixed phase clouds, the close proximity of the liquid clouds to the ice layers should be a reasonable test of the mixed phase retrieval accuracy.

[57] Another source of uncertainty is cirrus particle shape. This uncertainty is quantified by simulating observations from clouds containing four different randomly oriented particle shapes: hexagonal column, 4 bullet-rosette, 7 bullet-rosette, and a "stick-ball" irregular shape. These shapes are somewhat idealized, for example, hexagonal columns are normally horizontally oriented. Observations are simulated for two cases: (1) each cirrus cloud made of a single, randomly chosen particle shape, and (2) all clouds made of an equal mixture of the four shapes. The retrievals are performed with a database made for the equal mixture of shapes. Thus the retrievals for the first case have errors caused by particle shape, while those for the second case do not.

[58] Single scattering calculations are performed using the Discrete Dipole Approximation (DDA), detailed by *Evans et al.* [1998] and references therein. The column and rosette aspect ratios are from *Yang et al.* [2001]. The hexagonal column diameter d for length L (in μm) is $d = 5.916L^{0.5}$ for $L \geq 50$ μm and $d = L$ for $L \leq 40$ μm. The rosettes are composed of solid ice cylinders that project from the center at a maximum distance from each other and have diameter $d = 2.31L^{0.63}$, where L is the bullet length. The stick-ball shape is a cylinder with the same aspect ratio as a bullet, but with a sphere of diameter $0.3L$ on one end. The scattering properties are computed for 25 discrete particle sizes with maximum diameter from 10 μm to 2500 μm (1 dB intervals). The dipole sizes are 1/7, 1/4, and 1/6 the column or bullet diameter for the columns, rosettes, and stick-balls, respectively, with a minimum size of 5 μm. The single particle size scattering properties (extinction, single scattering albedo, and phase function) at each of the four center frequencies are combined for gamma size distributions with widths $\alpha = 0$ and $\alpha = 2$. To avoid too much truncation of the gamma size distributions in equivalent mass sphere diameters, the D_{me} range of the scattering table is limited from 25 to 500 μm. The equal particle shape mixture distribution has the same number concentration of each of the four particle shapes. Retrieval simulations are performed with parameters identical to the midlatitude winter scenario, but with the different particle scattering tables.

[59] The results of the nonspherical particle test are shown in Figure 13. The increased IWP retrieval error due to the particle shape effect is only noticeable for IWP > 30 g/m^2, but remains small. At lower IWP the error from particle shape is dominated by the other error sources such as instrument noise. The error probably continues to increase with IWP because larger IWP is associated with larger particle sizes which have a greater particle shape difference. This small particle shape effect is explained by the small differences in SWCIR brightness temperatures between the random single shape and equal mixture simulations. The rms brightness temperature difference is less than 1.0 K (the SWCIR noise level) in all ten channels, and 98% of the 643 GHz T_b differences are less than 1.0 K. The experiment may underestimate the particle shape errors because the retrieval is performed with the mean particle shape distribution,

Table 5. Ice Water Path and Median Mass Diameter Fractional Errors Over All Simulated Observations With IWP Greater Than 5 g/m^2[a]

Experiment	IWP dB Error		D_{me} dB Error	
	Median	rms	Median	rms
MLW[a], θ = 30°	1.1	2.3	0.7	1.3
MLW, θ = 70.5°	0.9	2.1	0.5	1.0
TRP, θ = 0°	1.1	2.4	0.6	1.1
TRP, θ = 70.5°	0.9	2.0	0.5	0.9

[a] MLW is the midlatitude winter simulation, and TRP is the tropical simulation. θ is the viewing zenith angle.

Table 6. Statistics on the Absolute Retrieval Error Normalized by the Bayes Retrieved Error Bars[a]

Simulation	Parameter	Fraction Valid	Fraction Within 1σ	Fraction Within 3σ
MLW	IWP	0.961	0.783	0.976
MLW	D_{me}	0.961	0.715	0.981
TRP	IWP	0.972	0.775	0.974
TRP	D_{me}	0.972	0.680	0.980

[a] The fraction of cases with valid error bars and the fraction of those with normalized errors between ±1 and ±3 are listed. Results are shown for the midlatitude winter (MLW) and tropical (TRP) simulations.

whereas realistically the particle shape mixture used in the retrieval algorithm would be biased compared to reality. On the other hand, a wide range of particle morphologies have been modeled, and real cirrus are almost always a mixture of shapes, rather than made of a single shape as assumed here.

[60] Up to this point the retrieval simulations have assumed that the prior distribution of profiles in the retrieval database had the same statistics as those of the simulated observations. For retrievals with actual SWCIR data the true cirrus microphysical statistics would not be known exactly. The effect of the retrieval database having incorrect statistics is explored by performing retrievals for the midlatitude winter simulation with a different database. The alternate midlatitude winter retrieval database is identical to the regular one except that (1) the CEPEX microphysics (Table 2) is assumed, and (2) the standard deviation of cloud top height is reduced from 1.5 to 1.0 km. The IWP and D_{me} retrieval accuracy for the two retrieval databases is compared in Figure 14. As expected, the retrievals with the alternate database have greater error. For IWP the median retrieval error is increased only by about 0.3 dB. The D_{me} error for the alternate retrieval database is much larger for the lower-altitude clouds. The CEPEX microphysics extrapolated to the higher temperatures of these low clouds results in much smaller D_{me} compared to the FIRE-I microphysics (median of 240 μm vs. 420 μm for Z_{top} < 4km). The water vapor screening of the lower-altitude clouds prevents the SWCIR channels from determining the particle size, so the Bayesian algorithm obtains the D_{me} information from the incorrect prior pdf.

5.3. Pixel Averaged Ice Cloud Retrieval Results

[61] One important use of SWCIR measurements will be to determine the average ice water path over an area to compare with numerical cloud modeling results or other remote sensing techniques. Averaging reduces the random retrieval errors and also the sampling errors. Sampling errors arise from estimating the mean of a population by measuring only some samples. For example, the SWCIR might be flown on several flight segments above a region with cirrus clouds, but would still sample only a small fraction of the columns in the region. Nevertheless, the mean ice water path might be well estimated if enough independent parts of the region

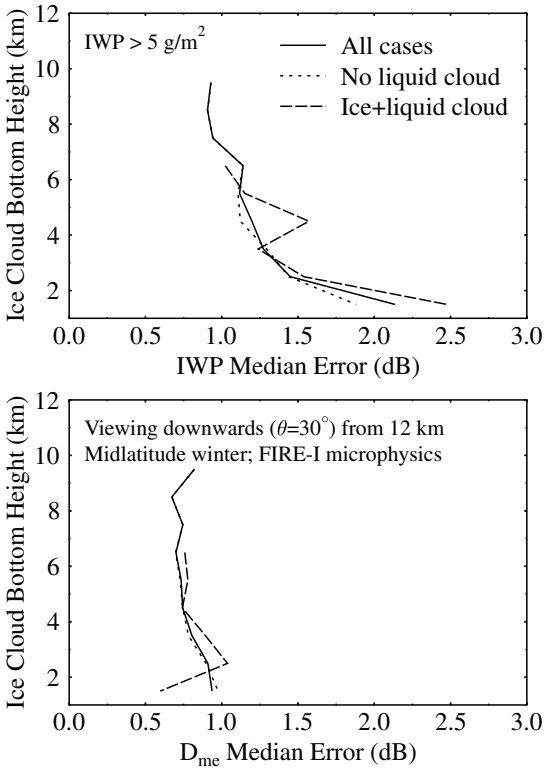

Figure 12. Median IWP and D_{me} error as a function of cloud bottom height for all cases in the midlatitude winter simulation, those with no liquid clouds, and those with both ice and liquid clouds.

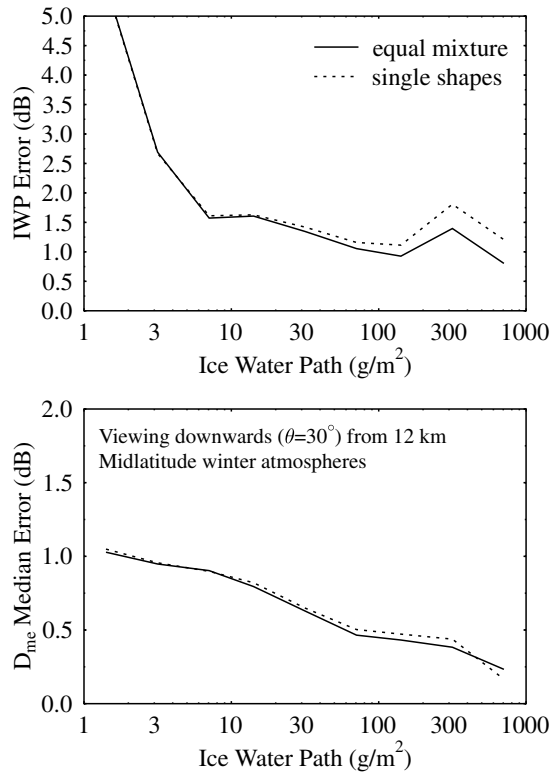

Figure 13. Median IWP and D_{me} error as a function of ice water path for observations simulated with (1) all clouds made from an equal mixture of four particle shapes, and (2) each cloud made of a single randomly selected shape.

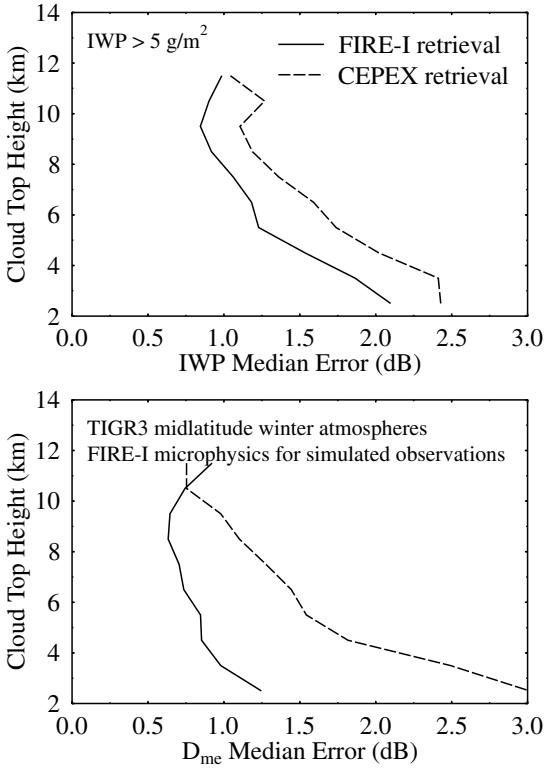

Figure 14. Median IWP and D_{me} error as a function of cloud top height for the midlatitude winter simulation, comparing retrievals done with the correct (FIRE-I) and incorrect (CEPEX) prior pdf retrieval databases.

were sampled. Successive pixels from the SWCIR will not be independent because ice clouds have spatial correlations extending tens to hundreds of kilometers.

[62] The sampling and retrieval errors are estimated in an experiment using the midlatitude winter simulation retrievals from the previous section. The questions asked are (1) how many independent samples must be averaged to reduce the sampling error to a desired level, and (2) how does the retrieval error compare with the sampling error? The $N = 10{,}000$ simulated cases are divided into N/M groups of M independent samples each. The sampling error is the rms of the difference between the mean true IWP in each group and the mean over all 10,000 cases. The retrieval error is the rms over the groups of the difference between the mean true IWP and mean retrieved IWP of each group. The retrieval error does not include the sampling error. The pixel averaged sampling and retrieval errors are absolute (not fractional) errors expressed in g/m^2.

[63] Figure 15 shows how the rms sampling and retrieval errors depend on the number of independent samples for the midlatitude winter simulation. The sampling error almost perfectly follows the expected $\sqrt{M}$ dependence. It is important to note that for single samples, the rms sampling error for ice water path is larger than the mean, 75 g/m^2 versus 30 g/m^2. For these simulated clouds it takes about 100 independent samples to reduce the sampling error to 25% of the mean. The retrieval error is shown for two sets of retrievals: one using the same FIRE-I microphysics as in the simulated observations and the other using the incorrect CEPEX microphysics (see discussion of Figure 14). The rms IWP retrieval error is comparable to the mean IWP for single pixel samples due to a few bad retrievals at high IWP that dominate the rms. The rms error for the retrievals with the correct cloud statistics remains well below the sampling error (for example, it is 9% of the mean IWP for 100 independent samples). In fact, it is a property of the Bayesian algorithm with the correct prior pdf that the retrieval error of the mean converges to zero. In the more reasonable scenario of the prior pdf not agreeing with the observed statistics, the retrieval error asymptotes with the number of independent samples. In this example, the CEPEX IWP retrieval error asymptotes to 8.5 g/m^2 after about 200 samples. Thus the sampling errors are important and will usually exceed the retrieval errors when small numbers of independent samples are averaged together.

5.4. Humidity Profile Retrieval Results

[64] While the main purpose of the SWCIR is not to retrieve water vapor, the water vapor channels necessary for accurate ice cloud retrievals may provide good retrievals of upper tropospheric humidity. The Bayesian algorithm can easily retrieve any parameter that is varied in the database, such as the temperature and water vapor profiles. The average temperature and integrated water vapor in 2 km thick layers were retrieved for the midlatitude winter and tropical simulations, including the ice clouds as described above. Table 7 lists the temperature and water vapor retrieval errors and the statistics of the original temperature and water vapor profiles.

[65] The simulated water vapor retrievals are very poor for the midlatitude winter experiment, with the rms retrieval errors being only slightly smaller than the standard deviation of the water vapor profile. This is probably because there is no source of temperature profile information. Water vapor retrievals for a downward viewing radiometer are highly sensitive to uncertainties in the temperature. In contrast, the water vapor retrievals for the upward viewing tropical experiment are quite good. The rms water vapor error in the 10–12 km layer is only 10% of the standard deviation and 6% of the mean water vapor amount. The absolute rms water vapor error is about the same for the 12–14 km layer, but the water vapor amount is about one fifth. The fractional errors for higher altitude tropical layers would be much worse, because there is much less water vapor (unless the aircraft flight level was higher so that the layers contributed significantly to the total integrated vapor). The temperature retrievals in the tropical experiment also reduce the uncertainty substantially. The good temperature and water vapor retrievals are explained by the upward viewing geometry. The atmosphere above 10 km is usually optically thin for most of the SWCIR frequencies. The measured brightness temperature is then proportional to the vertically integrated water vapor and the mean temperature. With two channels of different water vapor sensitivity, both temperature and integrated water vapor can be accurately retrieved. These simulations show that the SWCIR can measure

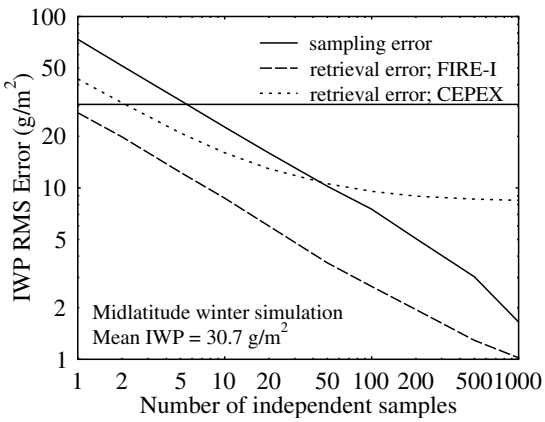

Figure 15. The RMS sampling and retrieval errors in ice water path for averaging a number of independent samples of the midlatitude winter simulated clouds. The pixel averaged retrieval error is shown for retrievals made with the correct statistics (FIRE-I) and the incorrect statistics (CEPEX). The mean IWP is shown with a line and listed in the lower left.

Table 7. SWCIR Simulated Retrieval Accuracy for Temperature and Water Vapor Amount[a]

Layer, km	Temperature, K			Water Vapor, g/m^2		
	Mean	s.d.	rms Error	Mean	s.d.	rms Error
			Midlatitude Winter Simulation			
12–10	219.9	5.61	4.69	12.48	12.02	10.94
10–8	224.8	4.48	3.53	54.74	53.22	42.02
8–6	235.4	6.22	4.06	255.3	227.2	182.6
6–4	247.9	7.63	4.44	847.6	695.6	573.3
			Tropical Simulation			
14–12	217.9	4.98	2.88	47.61	30.90	11.73
12–10	233.4	4.68	1.95	219.6	137.4	13.4

[a] SWCIR simulated retrieval accuracy for temperature and water vapor amount for the two simulations (downward viewing from 12 km in midlatitude winter and upward viewing from 10 km in the tropics). The mean and standard deviation of temperature and water vapor in the true atmospheres, and the rms retrieval error are listed.

water vapor above the flight altitude accurately even in the presence of cirrus clouds. The water vapor profile retrievals should be better if temperature profile information is available from radiosondes or numerical weather prediction models. The addition of temperature profile information is likely to make the downward viewing water vapor retrievals useable.

6. SWCIR Frequency Selection

[66] This section describes the simulation methods used to choose the SWCIR frequencies. These methods may be generally applicable to the design of heterodyne submillimeter radiometers for cirrus sensing. A previous submillimeter cirrus remote sensing article suggested a set of frequencies in atmospheric windows spaced by a factor of 1.3 to 1.4 apart [*Evans et al.*, 1998]. This recommendation was made before the role of water vapor screening and ice cloud vertical inhomogeneity in the retrieval process were fully appreciated. In general, there are two aspects to frequency selection: (1) the general configuration of receivers and number of channels, and (2) the exact placement of the band passes of the channels. The frequency selection approach recommended here is to select candidate sets of channels, tune the exact frequencies using clear-sky absorption considerations, and then perform retrieval simulations to determine the best set of frequencies for cirrus sensing. An iterative approach may be required.

[67] The initially selected SWCIR 183 GHz, 325 GHz, and 448 GHz receiver specifications were vetted by radiometer receiver engineers to produce a set of receiver specifications that could be realized within the available budget. Simulations were used to assess cirrus retrieval performance. The receiver specifications were then iterated between simulations and receiver engineering studies to optimize their cirrus retrieval performance.

6.1. Exact Frequency Selection

[68] Two procedures were performed to choose the exact bandpass frequencies of the SWCIR channels: (1) matching clear-sky transmission by minimizing brightness temperature differences between channels, and (2) examining clear-sky weighting functions to adjust the vertical sensitivity of the water vapor absorption line frequencies. Matching the clear-sky transmission reduces the effect of water vapor variability by making the frequencies equally sensitive to water vapor. The weighting functions are adjusted to obtain relatively independent information about the vertical profile.

[69] The clear-sky transmission profiles for the three lower frequencies are matched to that of the 643 GHz channel by finding the band passes that yield the closest brightness temperatures. The atmospheric profile of water vapor affects the matching due to the different pressure dependence of absorption at the four frequencies. The 643 and 448 GHz channels are in the wings of strong water vapor absorption lines (especially the 557 GHz line), while the 325 and 183 GHz channels are closer to the center of weak absorption lines. Owing to pressure broadening of the absorption lines, the water vapor absorption coefficient increases with pressure for 448 and 643 GHz at more than twice the rate as for the matched 183 and 325 GHz frequencies. Thus, in an atmosphere where the weighting function peak is at lower altitude (higher pressure), the 643 GHz absorption will be relatively greater than the 183 GHz channel absorption. A drier atmosphere has its weighting function peak at a lower altitude, hence the 183 and 325 GHz brightness temperatures will tend to be higher than those at 448 and 643 GHz. A moister atmosphere has its weighting function peak at a higher altitude, hence the 183 and 325 GHz brightness temperatures will tend to be lower than those at 448 and 643 GHz. For this reason, it is not possible to perfectly match the brightness temperatures under all conditions.

[70] The procedure to match the channel transmissions adjusted the frequencies to give the best brightness temperature match over 20 selected atmospheric profiles. To assure that the frequencies would match over a wide range of conditions expected for downward viewing with the SWCIR, 10 midlatitude summer and 10 midlatitude winter atmospheres were selected. The McClatchey standard atmosphere is used with nine chosen from the TIGR3 database of atmospheric profiles. The selected profiles had high upper troposphere relative humidity, so they would be likely to have cirrus clouds.

[71] The radiative transfer model used for this study is the same hybrid model described above. The molecular absorption is calculated with the LBLRTM model for 0.5 km layers at 0.03 GHz spectral resolution. The radiances calculated at this fine resolution are averaged over a rectangular band pass of 0.9 GHz for the transmission matching. Brightness temperatures are computed for nadir viewing from an altitude of 12 km. The matching frequencies are found by moving the channel offsets in 0.03 GHz steps. The criterion for the best match is the root mean square (rms) brightness temperature difference from 643 GHz over the 20 atmospheres.

[72] Table 8 lists the matched frequencies and the rms T_b error. As expected, the rms brightness temperature difference from 643 GHz is highest for the two channels on the weak absorption lines. These matching channels are fairly close to the absorption line center. Given the wide range of atmospheres used, the rms brightness temperature errors are relatively small.

Table 8. Best Matching Radiometer Frequencies

Wavenumber, cm^{-1}	Frequency, GHz	rms $T_b^{(i)} - T_b^{(643)}$, K
6.114 ± 0.049	183.31 ± 1.47	0.89
10.846 ± 0.050	325.15 ± 1.50	0.82
14.943 ± 0.240	448.00 ± 7.20	0.22
21.443 ± 0.217	642.86 ± 6.50	0.00

[73] The ozone absorption spectrum is considered in choosing the double sideband offset for the 643 GHz channel. For upward viewing, a brightness temperature spectrum shows several ozone lines in the 643 GHz receiver band pass. The 643 GHz channel offset is chosen so that a 2 GHz bandwidth avoids the ozone lines.

[74] The two other channels for each receiver are chosen by analyzing weighting functions. Moving the channels closer to the water vapor line center shifts the weighting function to higher altitude. Conversely, moving the channels further from the line center shifts the weighting function to lower altitude. These channels in addition to the four matched ones (183.31 ± 1.47, 325.15 ± 1.50, 448.00 ± 7.20, 642.86 ± 6.50 GHz) provide information about the water vapor profile and cloud height which improves the cirrus retrievals.

[75] The weighting functions depend very much on the particular water vapor profile. For illustration, the weighting functions for a clear-sky standard midlatitude winter atmosphere are shown in Figures 16 and 17. Weighting functions are generated assuming nadir viewing and a domain top of 20 km. The weighting functions for the four matched channels are shown in Figure 16. The 183 and 325 GHz weighting functions are significantly below the 448 and 643 GHz ones. Since the standard midlatitude winter atmosphere is one of the driest used in the transmission matching, the differences between the weak absorption line channels (183 and 325 GHz) and the strong absorption line channels (448 and 643 GHz) are the greatest.

[76] The 448 GHz absorption line is quite strong, and thus channels can be added closer to the line center to obtain higher altitude weighting functions. Technological constraints limited how close the SWCIR band passes could be made to the central receiver frequency, with the minimum for the 448 GHz receiver being 1.0 GHz. A channel further from the absorption line center gives only a slightly lower altitude weighting function due to the strong water vapor absorption around the line. In section 6.2 it is shown that the extra channels closer to the line center improve the retrieval of higher-altitude clouds by helping to correct for the water vapor screening problem. The frequencies are selected to have uniformly separated weighting functions. The 448 GHz weighting functions are shown in Figure 17.

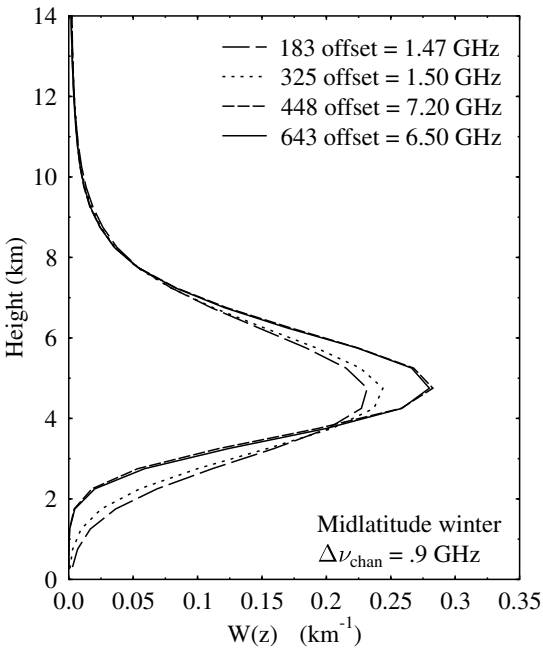

Figure 16. The weighting functions for the four transmission matched channels in a standard midlatitude winter atmosphere.

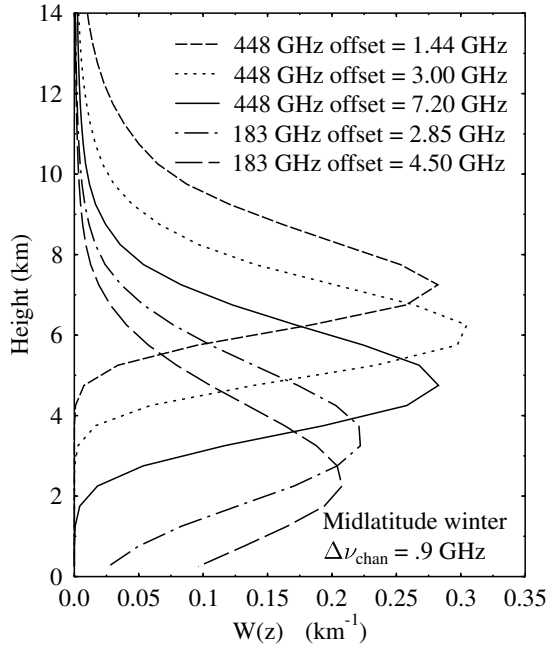

Figure 17. The weighting functions for the five levels sampled by the SWCIR frequencies for a standard midlatitude winter atmosphere.

[77] The 183 and 325 GHz absorption lines are too weak to allow channels closer to line center than the already selected matched channels. As a result, the extra channels on the 183 and 325 GHz lines provide lower altitude weighting functions. These channels allow retrieval of large ice particles (which can be sensed at these wavelengths) to lower altitudes than permitted by the 643 GHz weighting function. The 183 GHz channels are chosen to conform to the receiver specification of the maximum band pass of 5 GHz and to give evenly spaced weighting functions. The 325 GHz channel locations were matched to the 183 GHz ones by minimizing the brightness temperature error over the 20 atmospheres as described earlier. The 183 GHz weighting functions are shown in Figure 17.

[78] With the two higher-altitude channels on the 448 GHz receiver and the two lower-altitude channels on 183 and 325 GHz receivers, there are a total of five levels sensed by the SWCIR (weighting functions are shown in Figure 17). In a standard midlatitude winter atmosphere the weighting function peaks range from 2.4 km to 7.2 km. The weighting function peaks for the matched channels are approximately 4.8 km for the winter atmosphere and 6.6 km for the standard midlatitude summer atmosphere. Figure 18 shows the SWCIR channel center frequencies located on brightness temperature spectra plots.

6.2. Retrieval Simulations for Frequency Configurations

[79] Ice cloud retrieval simulations as described in section 5.1 are performed for a number of frequency configurations. To simplify the description, results are shown for only four configurations using the final set of SWCIR frequencies. Table 9 lists the exact frequencies for the four configuration experiments. The last entry is the full set of frequencies chosen for the SWCIR.

[80] The key results are shown in Figure 19 which plots the rms retrieval error for the midlatitude winter simulation as a function of cloud top height for the four frequency configurations. Starting with the 643 GHz plus 448 GHz configuration (1), there is only a modest improvement in IWP retrieval accuracy when adding the lower frequencies of configuration 2 with a single matched band pass at all four frequencies. There is a substantial improvement in

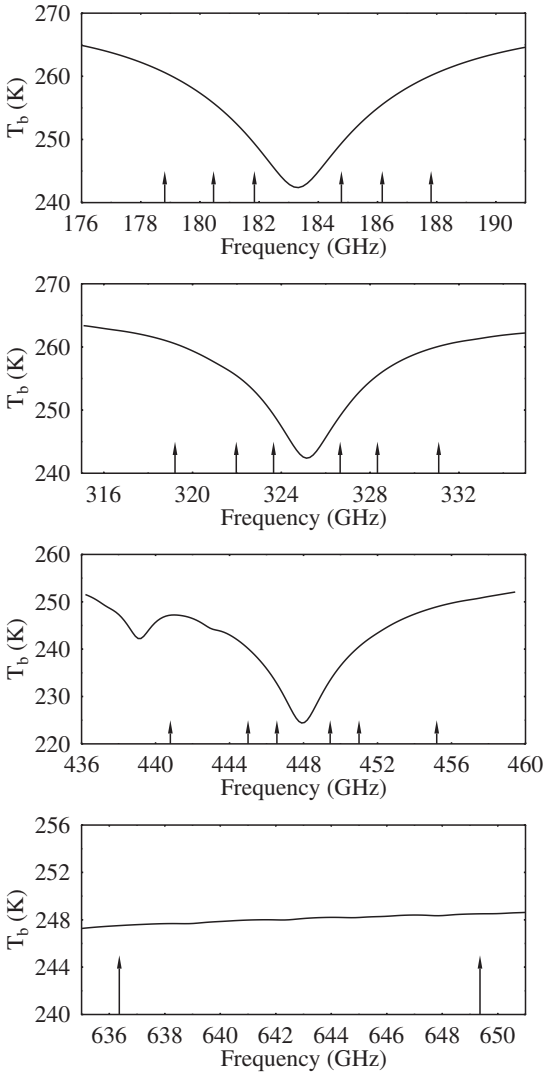

Figure 18. Brightness temperature spectra for the four SWCIR receivers for nadir viewing in a standard midlatitude winter atmosphere. The center locations of the 10 double sideband channels are shown with arrows.

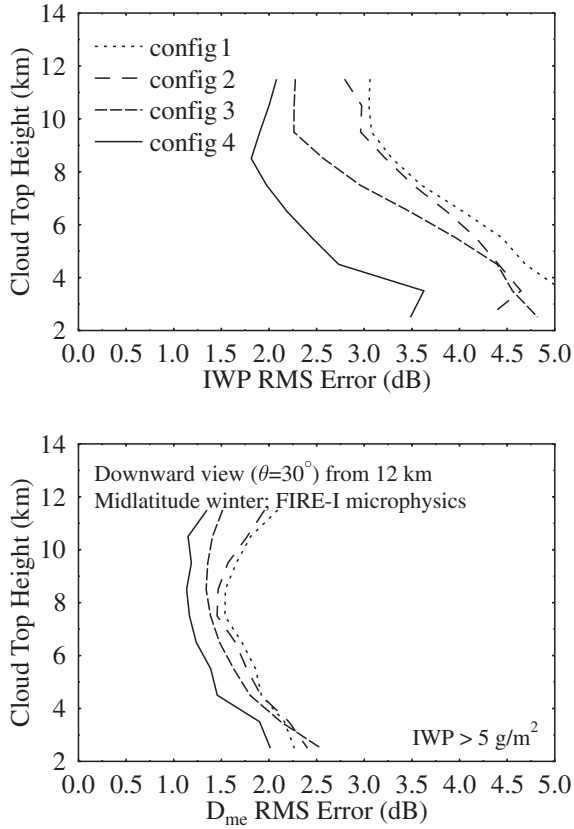

Figure 19. RMS IWP and D_{me} error as a function of cloud top height for four sets of SWCIR frequencies. The configurations are listed in Table 9.

the retrieval of higher-altitude clouds with the addition of the other two 448 GHz receiver frequencies. This is a result of the ability to measure the amount of water vapor in and above the high-altitude clouds. The addition of the lower-altitude frequencies of the 325 GHz and 183 GHz receivers dramatically improves the IWP retrievals, especially for lower-altitude clouds. These channels are less sensitive to water vapor, and hence are able to sense the lower-altitude ice clouds. They also provide information on the upwelling radiance in thick ice clouds, which improves the retrievals of some high-altitude clouds.

Table 9. Frequency Configurations for the Retrieval Simulations

Configuration	Frequencies, GHz
1	448.00 ± 7.20, 642.86 ± 6.50
2	183.31 ± 1.47, 325.15 ± 1.50, 448.00 ± 7.20, 642.86 ± 6.50
3	183.31 ± 1.47, 325.15 ± 1.50, 448.00 ± 1.44, ±3.00, ±7.20, 642.86 ± 6.50
4	183.31 ± 1.47, ±2.85, ±4.50, 325.15 ± 1.50, ±3.18, ±5.94, 448.00 ± 1.44, ±3.00, ±7.20, 642.86 ± 6.50

[81] Figures 20 and 21 show the retrieval error for the four frequency configurations as a function of ice water path for the midlatitude winter and tropical simulations. In the midlatitude winter simulation the IWP error is similar for all four configurations for the 10 to 50 g/m^2 range, but substantially different for lower and higher IWP. The largest improvement comes with the addition of the lower-altitude 325 GHz and 183 GHz frequencies because most of the high IWP clouds in this simulation are at low altitudes that the other frequencies cannot sense well. In the tropical simulation there is a significant improvement in configuration 2 over configuration 1, especially in the D_{me} retrieval. However, there is almost no further improvement with the addition of the other six frequencies. The tropical simulation assumes an upward view from 10 km, so the lower water vapor absorption of the additional 325 GHz and 183 GHz frequencies does not help. The total water vapor information provided by the matched 183 GHz frequency is apparently adequate for the IWP retrievals. The upward viewing geometry underneath tropical cirrus is a much simpler retrieval problem due to the cold uniform background of space and the reduction in water vapor absorption.

7. Summary and Conclusions

[82] This paper provides a comprehensive analysis of the use of discrete frequency submillimeter radiometers to retrieve ice water path and characteristic particle size of ice clouds. This technique is important for enabling spaceborne measurements of cirrus proper-

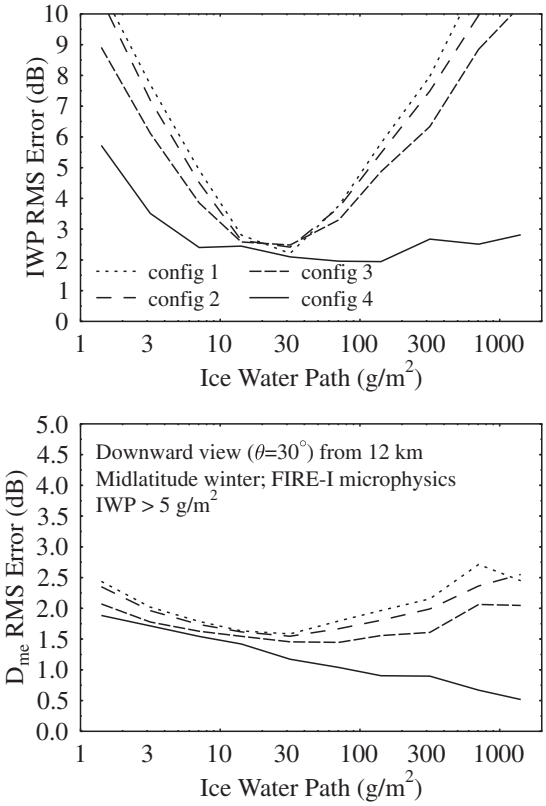

Figure 20. RMS IWP and D_{me} error from the midlatitude winter simulation as a function of ice water path for four sets of SWCIR frequencies. The configurations are listed in Table 9.

ties, meeting key climate modeling and NASA measurement needs.

[83] The JPL Submillimeter-Wave Cloud Ice Radiometer has ten channels centered about four receivers at 183, 325, 448, and 643 GHz. The SWCIR will view out a side window of the NASA DC-8 and scan from zenith to near nadir. This paper describes the retrieval algorithm developed for the SWCIR, an ice cloud retrieval simulation system, results of the retrieval accuracy from the simulations, and the rationale for choosing the SWCIR frequencies.

[84] A Bayesian algorithm is used to retrieve primarily ice water path (IWP) and median mass equivalent sphere diameter (D_{me}). This algorithm combines prior information about cirrus clouds and atmospheric properties with radiative transfer simulations to retrieve ice cloud parameters. The retrieved parameter vector is the mean of the posterior probability density function. A large precalculated database of random ice clouds and atmospheric profiles and corresponding simulated SWCIR brightness temperatures is input to the algorithm. The technique efficiently integrate over only those database points that are close to the observed brightness temperatures, resulting in fast retrievals.

[85] A new method is presented for generating clouds for the database and retrieval simulations. This procedure makes ice clouds with realistic properties using statistics from a large amount of in situ ice cloud microphysical data. The input microphysical data were measured by 2-D probes flown in the FIRE-I experiment for midlatitude winter ice clouds and CEPEX for tropical cirrus anvils. The method consists of using the observed statistics and correlations between temperature, particle size, and ice water content. Stochastic profiles of temperature and relative humidity are made with statistics from a standard radiosonde data set. Random cloud heights and thicknesses having reasonable distributions are generated. The cloud top and base temperature are then used to select cloud top and bottom ice water content and particle size using the observed statistics. The internal cloud properties are interpolated from the base and top IWC and particle size. If the cloud base is below a randomly chosen ice-to-liquid transition zone, then it consists of an ice layer above a liquid layer.

[86] Retrieval experiments were performed for midlatitude winter ice clouds with the SWCIR viewing downward from 12 km and for tropical anvil cirrus with the SWCIR viewing upward from 10 km. For midlatitude winter ice clouds with IWP greater than 5 g/m^2, the overall median fractional error for zenith viewing is 1.1 dB for IWP and 0.7 dB for D_{me} (this means that 50% of the IWP retrievals are within 30%), while for tropical cirrus the median error is 1.1 dB for IWP and 0.6 dB for D_{me}. While many cirrus clouds have IWP less than 5 g/m^2, 97% of the simulated ice mass are in clouds with IWP greater than 5 g/m^2.

[87] For the downward viewing midlatitude winter simulation, the retrieval errors increase for lower altitude clouds due to water vapor screening, but not dramatically so because the 183 and 325 GHz channels can sense the larger ice particles present in lower-altitude clouds. For the upward viewing tropical simulation, the retrieval errors increase for higher-altitude clouds due to the small particles and low IWP characteristics of very cold cirrus. The effect of liquid clouds just below ice clouds in the midlatitude winter simulation is quite small. The particle shape issue is addressed by simulating SWCIR brightness temperatures for randomly oriented hexagonal columns, bullet-rosettes, and irregular particles. Retrieval simulations show that the particle shape errors are quite small compared to the other errors.

[88] Retrieval simulations also demonstrated that the SWCIR can provide accurate water vapor measurements in two 2 km thick layers above an assumed flight altitude of 10 km in tropical anvil cirrus. The rms error in water vapor in the 10–12 km layer is 6% of the mean, while for the 12–14 km layer it is 25% of the mean. The SWCIR downward viewing water vapor retrievals are very poor,

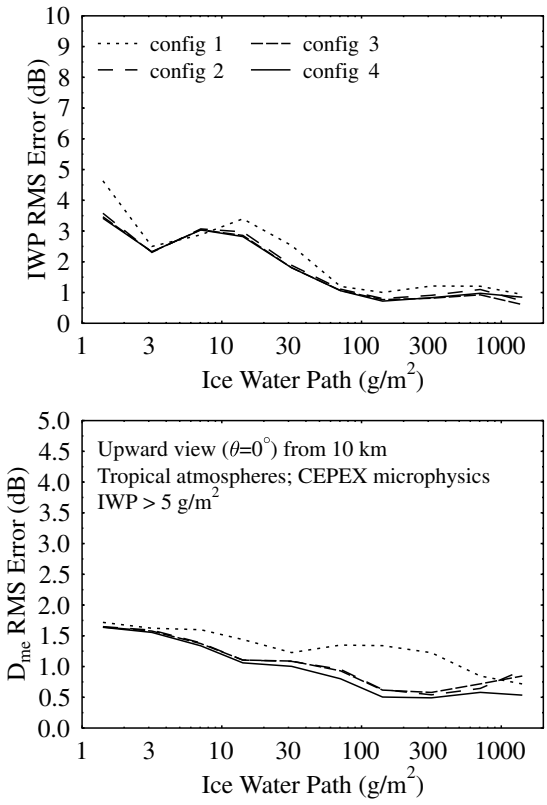

Figure 21. RMS IWP and D_{me} error from the tropical simulation as a function of ice water path for four sets of SWCIR frequencies. The configurations are listed in Table 9.

which we believe is due to the lack of temperature information. Radiometer frequencies on oxygen absorption lines or external sources of temperature information would improve the water vapor profile retrievals.

[89] The results of these simulations depend on the particular ice cloud microphysics data used and the cloud geometry parameters assumed. These are meant to be realistic, but do not apply to all cirrus. The issue of variable surface emissivity was not considered. The surface will seldom be sensed by most of the SWCIR channels, but the lower-altitude channels will certainly detect the surface in drier (e.g., cold winter) atmospheres. The issue of nonspherical ice particles was addressed briefly, and a more comprehensive approach to estimating the particle shape error is warranted. The use of polarization for retrieving information about particle shape was also left for future exploration.

[90] The procedure described for selecting radiometer frequencies can be divided into two parts: (1) determining the general configuration of receivers and channels using retrieval simulations and (2) determining the exact receiver band passes from clear-sky atmospheric absorption characteristics. Several candidate sets of frequencies are chosen from the possibilities allowed by receiver technology and the following general considerations. The receivers should be located at relatively equal multiples of frequencies, e.g., factors of 1.4, on absorption lines so that the atmospheric transmission may be matched across the spectrum. By locating a central receiver frequency at an absorption line, several channels with varying absorption characteristics may be obtained inexpensively. The absorption lines should be weak enough, however, that high atmospheric transmission is still accessible using a frequency as far as practical from the line center (i.e., equivalent to an atmospheric window).

[91] The exact frequencies of the candidate sets may be determined by considering their clear-sky transmission characteristics. The first principle is to match the atmospheric transmission of channels across the spectrum by matching simulated brightness temperatures over a suitably wide range of atmospheres. The second principle is to tune the multiple frequencies of a receiver so that the weighting functions are sensitive to a range of atmosphere heights.

[92] Once the candidate frequencies are chosen, retrieval simulations are performed for all frequency sets. These simulations should include a broad range of ice cloud and atmospheric properties and instrument situations (e.g., viewing angles and flight altitudes). The frequency set with the best retrieval performance can then be chosen. For the SWCIR we found that frequencies closer to the 448 GHz line center (with higher-altitude weighting functions) substantially improved the downward viewing retrieval of high-altitude cirrus. The frequencies further from the 183 GHz and 325 GHz line centers, with lower-altitude weighting functions, dramatically improved the retrievals of low-altitude midlatitude winter ice clouds, which have large particles and high IWP.

[93] We believe the ideal submillimeter radiometer for cirrus and upper tropospheric water vapor sensing would have receivers centered on both water vapor and oxygen absorption lines and include frequencies up to about 900 GHz. Above 900 GHz the upper troposphere starts to become too opaque for cirrus measurement. There are suitable oxygen lines at 118, 425, 487, and 834 GHz. Appropriate water vapor lines exist at 183, 325, 380, 448, 621, and 916 GHz. The 621 GHz line is not in the center of the 600–700 GHz window, so a window frequency around 663 GHz might also be useful. For example, two candidate sets of frequencies are 183, 325, 448, 620, 834 GHz and 183, 380, 487, 663, 916 GHz. Clearly, more frequencies are better, but there are economic constraints. There are also technical constraints, such as (1) the bandwidth required for a given receiver noise temperature and desired integration time, (2) the minimum and maximum frequencies allowed from the central receiver frequency, and (3) the maximum local oscillator frequency for room temperature receivers. The best choice of frequencies will depend on the particular retrieval requirements and should be determined with appropriate retrieval simulations.

[94] **Acknowledgments.** Aaron Evans wrote preliminary versions of the retrieval and simulation codes and performed some of the initial simulations. The work was funded by contract 1211073 from the Jet Propulsion Laboratory, California Institute of Technology, to the University of Colorado. The SWCIR development was funded by a contract from the NASA Instrument Incubator Program to the Jet Propulsion Laboratory.

References

Bernardo, J. M., and A. F. M. Smith, *Bayesian Theory*, John Wiley, New York, 1994.

Chedin, A., Improved initialization inversion method: A high-resolution physical method for temperature retrievals from satellites of the TIROS-N series, *J. Clim. Appl. Meteorol.*, *24*, 128–143, 1985.

Deeter, M. N., and K. F. Evans, A hybrid Eddington-single scattering radiative transfer model for computing radiances from thermally emitting atmospheres, *J. Quant. Spectrosc. Radiat. Transfer*, *60*, 635–648, 1998.

Deeter, M. N., and K. F. Evans, A novel ice-cloud retrieval algorithm based on the millimeter-wave imaging radiometer (MIR) 150- and 220-GHz channels, *J. Appl. Meteorol.*, *39*, 623–633, 2000.

Del Genio, A. D., M.-S. Yao, W. Kovari, and K. K.-W. Lo, A prognostic cloud water parameterization for global climate models, *J. Clim.*, *9*, 270–304, 1996.

Evans, K. F., and G. L. Stephens, Microwave radiative transfer through clouds composed of realistically shaped ice crystals, part II, Remote sensing of ice clouds, *J. Atmos. Sci.*, *52*, 2058–2072, 1995.

Evans, K. F., S. J. Walter, A. J. Heymsfield, and M. N. Deeter, Modeling of submillimeter passive remote sensing of cirrus clouds, *J. Appl. Meteorol.*, *37*, 184–205, 1998.

Fowler, L. D., D. A. Randall, and S. A. Rutledge, Liquid and ice cloud microphysics in the CSU General Circulation Model, part I, Model description and simulated microphysical processes, *J. Clim.*, *9*, 489–529, 1999.

Gasiewski, A. J., Numerical sensitivity analysis of passive EHF and SMMW channels to tropospheric water vapor, clouds, and precipitation, *IEEE Trans. Geosci. Remote Sens.*, *30*, 859–870, 1992.

Gatti, M. S., S. R. Stewart, J. G. Bowen, and E. B. Paulsen, A radio telescope for the calibration of radio sources at 32 gigahertz, *TDA Prog. Rep. 42-118*, Jet Propul. Lab., Pasadena, Calif., 1994.

Giraud, V., J. C. Buriez, Y. Fouquart, F. Parol, and G. Seze, Large-scale analysis of cirrus clouds from AVHRR data: Assessment of both a microphysical index and the cloud-top temperature, *J. Appl. Meteorol.*, *36*, 664–675, 1997.

Heymsfield, A. J., K. M. Miller, and J. D. Spinhirne, The 27-28 October 1986 FIRE IFO cirrus case study: Cloud microstructure, *Mon. Weather Rev.*, *118*, 2313–2328, 1990.

Heymsfield, A. J., S. Lewis, A. Bansemer, J. Iaquinta, M. Kajikawa, C. Twohy, and M. R. Poellot, A general approach for deriving the properties of cirrus and stratiform ice cloud particles, *J. Atmos. Sci.*, in press, 2002.

Johnson, L. H., Broadband polarization rotator for the infrared, *Appl. Opt.*, *16*, 1082–1084, 1977.

Liu, G., and J. A. Curry, Determination of ice water path and mass median particle size using multichannel microwave measurements, *J. Appl. Meteorol.*, *39*, 1318–1329, 2000.

Lohmann, U., and E. Roeckner, Design and performance of a new cloud microphysics scheme developed for the ECHAM general circulation model, *Clim. Dyn.*, *12*, 557–572, 1996.

McFarquhar, G. M., and A. J. Heymsfield, Microphysical characteristics of three anvils sampled during the central equatorial Pacific experiment, *J. Atmos. Sci.*, *53*, 2401–2423, 1996.

Minnis, P., P. W. Heck, and D. F. Young, Inference of cirrus cloud properties using satellite-observed visible and infrared radiances, part II, Verification of theoretical cirrus radiative properties, *J. Atmos. Sci.*, *50*, 1305–1322, 1993.

Mizuno, H., T. Matsuo, M. Murakami, and Y. Yamada, Microstructure of cirrus clouds observed by hyvis, *Atmos. Res.*, *32*, 115–124, 1994.

Murakami, M., and T. Matsuo, Development of hydrometeor video sonde, *Ann. Meteorol.*, *25*, 144–147, 1988.

Ou, S. C., K. N. Liou, W. M. Gooch, and Y. Takano, Remote sensing of cirrus cloud parameters using advanced very-high-resolution radiometer 3.7- and 10.9- channels, *Appl. Opt.*, *32*, 2171–2180, 1993.

Racette, P., R. F. Adler, J. R. Wang, A. J. Gasiewski, D. M. Jackson, and D. S. Zacharias, An airborne millimeter-wave imaging radiometer for cloud,

precipitation, and atmospheric water vapor studies, *J. Atmos. Oceanic Technol.*, *13*, 610–619, 1996.

Rasch, P. J., and J. E. Kristjansson, A comparison of the CCM3 model climate using diagnosed and predicted condensate parameterizations, *J. Clim.*, *11*, 1587–1614, 1998.

Rolland, P., K. N. Liou, M. D. King, S. C. Tsay, and G. M. McFarquhar, Remote sensing of optical and microphysical properties of cirrus clouds using Moderate-Resolution Imaging Spectroradiometer channels: Methodology and sensitivity to physical assumptions, *J. Geophys. Res.*, *105*, 11,721–11,738, 2000.

Rossow, W. B., and R. A. Schiffer, Advances in understanding clouds from ISSCP, *Bull. Am. Meteorol. Soc.*, *80*, 2261–2287, 1999.

Rotstayn, L. D., A physically based scheme for the treatment of stratiform clouds and precipitation in large-scale models, part I, Description and evaluation of the microphysical processes, *Q. J. R. Meteorol. Soc.*, *123*, 1227–1282, 1997.

Siegel, P. H., I. Mehdi, R. J. Dengler, T. H. Lee, D. A. Humphrey, A. Pease, R. Zimmermann, and P. Zimmermann, A 640 GHz planar-diode fundamental mixer/receiver, in *Proceedings of MTT-S International Microwave Symposium, Baltimore, Maryland*, pp. 407–410, Inst. of Electr. and Electr. Eng., New York, 1998.

Sivia, D. S., *Data Analysis: A Bayesian Tutorial*, Clarendon, Oxford, England, 1996.

Smith, R. N. B., A scheme for predicting layer clouds and their water content in a general circulation model, *Q. J. R. Meteorol. Soc.*, *116*, 435–460, 1990.

Starr, D. O., and D. P. Wylie, The 27-28 October 1986 FIRE cirrus case study: Meteorology and clouds, *Mon. Weather Rev.*, *118*, 2259–2287, 1990.

Stubenrauch, C., R. Holz, A. Chedin, D. L. Mitchell, and A. J. Baran, Retrieval of cirrus ice crystal sizes from 8.3 and 11.1 micron emissivities determined by the improved initialization inversion of TIROS-N Operational Vertical Sounder observations, *J. Geophys. Res.*, *104*, 793–808, 1999.

Sud, Y. C., and G. K. Walker, Microphysics of clouds with the relaxed Arakawa-Schubert scheme (McRAS), part I, Design and evaluation with GATE Phase III data, *J. Atmos. Sci.*, *56*, 3196–3220, 1999.

Vanek, M. D., et al., Far infrared sensor for cirrus (FIRSC): An aircraft-based FTS to measure the earth radiance spectrum, *Appl. Opt.*, *40*, 2169–2176, 2001.

Wang, J., G. Liu, J. Spinhirne, P. Racette, and W. Hart, Observations and retrievals of cirrus cloud parameters using multichannel millimeter-wave radiometric measurements, *J. Geophys. Res.*, *106*, 15,251–15,263, 2001.

Warren, S. G., Optical constants of ice from the ultraviolet to the microwave, *Appl. Opt.*, *23*, 1206–1225, 1984.

Waters, J. W., et al., The UARS and EOS microwave limb sounder (MLS) experiments, *J. Atmos. Sci.*, *56*, 194–218, 1999.

Weng, F., and N. C. Grody, Retrieval of ice cloud parameters using a microwave imaging radiometer, *J. Atmos. Sci.*, *57*, 1069–1081, 2000.

Wielicki, B. A., R. D. Cess, M. D. King, D. A. Randall, and E. F. Harrison, Mission to Planet Earth: Role of clouds and radiation in climate, *Bull. Am. Meteorol. Soc.*, *76*, 2125–2153, 1995.

Yang, P., B.-C. Gao, B. A. Baum, Y. X. Hu, W. J. Wiscombe, S.-C. Tsay, D. M. Winker, and S. L. Nasiri, Radiative properties of cirrus clouds in the infrared (8-13 um) spectral region, *J. Quant. Spectrosc. Radiat. Transfer*, *70*, 473–504, 2001.

K. F. Evans, Program in Atmospheric and Oceanic Sciences, University of Colorado, 311 UCB, Boulder, CO 80309, USA. (evans@nit.colorado.edu)

A. J. Heymsfield and G. M. McFarquhar, National Center for Atmospheric Research, Boulder, CO 80305, USA.

S. J. Walter, Aerojet, 1100 West Hollyvale St., Azusa, CA 91702, USA.